IMPROVING ALIGNMENT OF KINEMATICALLY COUPLED POLYMER MICROFLUIDIC MODULES BY MODULARIZATION OF COUPLING FEATURES

by

Joseph E. Miller, B.S.T.

A thesis submitted to the Graduate Council of
Texas State University in partial fulfillment
of the requirements for the degree of
Master of Science
with a Major in Engineering
August 2020

Committee Members:

Namwon Kim, Chair

Byoung Hee You, Co-Chair

Jitendra Tate

FAIR USE AND AUTHOR'S PERMISSION STATEMENT

Fair Use

Duplication Permission

ACKNOWLEDGMENTS

My thanks to Boston Micro Fabrication for making the parts necessary for this research.

I would like to thank my thesis advisor Dr. Namwon Kim, committee member Dr. Jitendra Tate, and graduate advisor Dr. Vishu Viswanathan for their support and advice for my research.

Dr. Devanda Lek, once my professor, then lab mate, and now friend, has shown continued support throughout the program for which I am very appreciative. He led by example while completing his dissertation, and he seemingly never tired of my endless questions.

Most of all, I want to specially thank Dr. Byoung Hee You for guiding me through this journey. His mentorship in both engineering and life will have a lasting effect on me, and I cannot overstate the insight he has provided. He has my deepest gratitude for giving me this opportunity to expand my knowledge and contribute to the research community.

TABLE OF CONTENTS

Page

LIST OF TABLES

Table **Page**

LIST OF FIGURES

Figure **Page**

LIST OF ABBREVIATIONS

Abbreviation	Description
DNA	Deoxyribonucleic Acid
PMMA	Poly(methyl methacrylate)
PC	Polycarbonate
PDMS	Polydimethylsiloxane
θ_X	Assembly variable Rotation X; rotation of the upper module about the x-axis
θ_Y	Assembly variable Rotation Y; rotation of the upper module about the y-axis
θ_Z	Assembly variable Rotation Z; rotation of the upper module about the z-axis
X	Assembly variable Translation X; translation of the upper module along the x-axis
Y	Assembly variable Translation Y; translation of the upper module along the y-axis
Z	Assembly variable Translation Z; translation of the upper module along the z-axis

T_{UM}^{LM}	Transformation matrix from the origin of the lower module to the origin of the upper module
$P_{H_i}^{UM}$	Vector from the origin of the upper module to the center of post hemisphere i
$P_{CP_i}^{LM}$	Vector from the origin of the lower module to contact point i
$n_{CP_i}^{LM}$	Normal vector from the surface of the v-groove to the center of the hemisphere
D_{H_i}	Diameter of hemisphere i
${}^{x}n_{CP_i}^{LM}$	X-coordinate of the normal vector
${}^{y}n_{CP_i}^{LM}$	Y-coordinate of the normal vector
${}^{z}n_{CP_i}^{LM}$	Z-coordinate of the normal vector
x_{CP_i}	X-coordinate of contact point i
y_{CP_i}	Y-coordinate of contact point i
z_{CP_i}	Z-coordinate of contact point i
${}^{x}P_{S_i}^{LM}$	X-coordinate of vector from the origin of the lower module to a point on v-groove surface i
${}^{y}P_{S_i}^{LM}$	Y-coordinate of vector from the origin of the lower module to a point on v-groove surface i

$^{z}P_{S_i}^{LM}$	Z-coordinate of vector from the origin of the lower module to a point on v-groove surface i
MATLAB	Matrix Laboratory; computing environment and programming language developed by MathWorks
Micron	Micrometer; metric unit of measure equal to 0.001 millimeters
µm	Micrometer
mm	Millimeter; metric unit of measure equal to 0.001 meters
$[J]$	Jacobian matrix
d_j	Component dimension j
PC_{ij}	Percent contribution of component dimension j to the variation of assembly variable i
s_{ij}	Sensitivity of dimension j to assembly variable i
t_j	Tolerance of component dimension j
TC_j	Total contribution of component dimension j
F_i	Correction factor for assembly variable i
$[C_A]$	Assembly variable covariance matrix

$[C_d]$	Component dimension covariance matrix
σ	Sigma; standard deviation
M_{xy}	Functional feature misalignment in the x-y plane
M_z	Functional feature misalignment in the z-axis direction
D	Distance from the center of the module to a functional feature
D_x	X-coordinate of a functional feature
D_y	Y-coordinate of a functional feature
t_{θ_X}	Tolerance for assembly variable Rotation X
t_{θ_Y}	Tolerance for assembly variable Rotation Y
t_{θ_Z}	Tolerance for assembly variable Rotation Z
BMF	Boston Micro Fabrication
PμSL	Projection Micro-Stereolithography

ABSTRACT

Mass production of affordable microfluidic devices is a subject of importance to the biological and medical communities. If devices are cheap enough to be disposable, tests can be run at a higher rate and lower cost without concern for contamination. Achieving this cost-effectiveness requires devices to be of polymer material, made by injection molding or hot embossing. Though these manufacturing processes provide high throughput, accuracy of the features is a concern. Features of particular interest are those used for alignment of device modules in the event devices are stacked to perform a series of functions. A kinematic coupling was previously introduced as a method of passive alignment of microfluidic device modules. The coupling involves a set of three hemisphere-tipped posts and three v-grooves to provide exact constraint of the modules using six contact points, two for each post-groove connection. The objective this research is to provide guidelines for improving the alignment of kinematically coupled devices and to explore a method of doing so on microfluidic device modules. Sensitivity analysis was performed on the kinematic coupling dimensions of injection molded microfluidic modules to identify the main causes of misalignment. The results indicate that the height and angularity of the hemisphere-tipped posts are the dimensions with the greatest effect on the alignment of two modules. Therefore, the proposed method of improving the alignment is to manufacture the posts separately by additive manufacturing, and then connect them to an injection molded device module. Misalignment of functional features such as aligned through-holes was used to characterize the effect of variation in the six

degrees of freedom. Monte Carlo simulations were used to show the reduction in functional feature misalignment depending on the reduction in component dimension tolerances. The maximum reduction in worst-case x-y plane misalignment possible by the proposed method is 22 percent. Maximum reduction in z-direction misalignment when decreasing only post dimension tolerances is 51 percent. However, simulations showed significant benefit to also decreasing groove dimension tolerances. When both are considered and set to ±2 μm, the maximum z-direction reduction rises to 80 percent. Hemisphere-tipped posts were additively manufactured by Boston Micro Fabrication using projection micro-stereolithography. The measurements of the post dimensions produced a maximum tolerance of ±1.3 μm, which is a 91 percent reduction from the tolerance of the same dimension on injection molded modules. If precision can be maintained throughout connection of the posts to the modules, the worst-case z-direction functional feature misalignment can be reduced by at least 51 percent and the x-y plane misalignment by 22 percent.

1. INTRODUCTION

1.1 Problem Statement

Sensitivity analysis was performed on kinematically coupled microfluidic modules using measurements from injection molded samples. The analysis will be discussed in detail in the next chapter. The results showed that the height and angularity of the hemisphere-tipped posts are the highest contributing dimensions to overall misalignment between two modules. This is partially due to the actual sensitivity of those dimensions and partially because they had the highest measured variation. For this reason, the features of focus in this research are the hemisphere-tipped posts.

It is common for the posts to experience defects from short shot or voids since they would likely be the last features in the mold to fill completely. However, short shot may be largely mitigated by adjusting mold temperature and injection speed, and voids can be prevented by proper venting or inducing vacuum in the mold cavity [1]. Another cause of dimensional inaccuracy of the posts can be structure deformation during demolding. This was observed in injection molded modules by You et al. (2015). The posts were angled and elongated past the nominal value which was surmised to be caused by the adhesion force between the polymer and the mold wall [2]. Low surface energy coatings can be applied to the mold surfaces before processing to mitigate this force, but devices used for biomedical purposes often have restrictions on the type of chemicals they can be exposed to [1]. Modularizing the posts by creating them separately and later assembling them with the microfluidic module is the proposed solution to this problem of hemisphere-tipped post deformation. The most promising method of manufacturing the posts is additive manufacturing. This will be discussed in detail in later chapters.

1.2 Background

Kinematic couplings are a method of achieving exact constraint between two assembled objects. They restrict the six degrees of freedom without over-constraint. An over constrained assembly can lead to unpredictable location and residual stresses [2]. The contact points between the coupling features can be mathematically determined, which makes the location of the objects known in relation to each other. They can be used to achieve precise, passive alignment of two or more objects with some functional relationship. A kinematic coupling in the form of three hemisphere-tipped posts and three v-grooves has been suggested to align stacked microfluidic device modules [3].

Microfluidic devices have become an important tool for biological and chemical analyses. They allow researchers to take advantage of the physical phenomena present at the micro scale while limiting use of expensive reagents. There are a wide variety of applications including DNA analysis, molecular diagnostics, water monitoring, alternative energy research, and cancer diagnosis [4], [5]. Stacking modules that each perform a separate function enables the customization of analyses. Passive alignment of the modules can be provided by a kinematic coupling. However, the coupling features must be accurately replicated to achieve proper functionality. Glass and silicon microfluidic devices can be fabricated with extreme accuracy by methods borrowed from the semiconductor industry such as photolithography and etching [6]. However, these materials and the production methods are expensive with low production volumes. Contamination between analyses, testing cost, and testing availability demand affordable devices, to the point of disposability [7]. Polymers such as PMMA, PC, and PDMS can be used to lower the material cost. Injection molding the modules provides capacity for

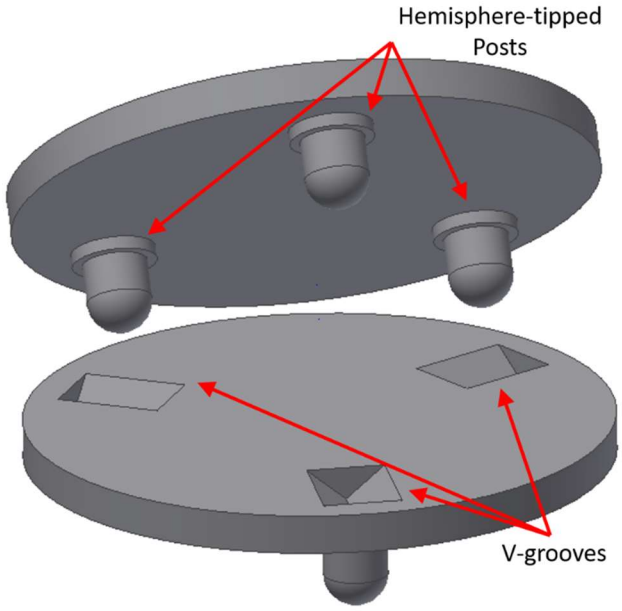

Figure 1. Kinematic Coupling. Autodesk Inventor model of an exaggerated kinematic coupling with hemisphere-tipped posts and v-grooves.

mass production [8], [9]. The drawback for this method of production is the challenge of quality control.

Manufacturing microfluidic devices by injection molding is inherently difficult because of the size of the features. The high surface area to volume ratio at the microscale leads to extreme heat loss and friction between the polymer and mold surface. These effects induce the requirements of temperatures, pressure, and injection speed to be higher than for conventional injection molding [10]. Common defects include short shots, sink marks, voids, weld lines, and structure deformation.

There has been vast improvement in additive manufacturing technologies over the past few decades, leading to the development of a wide variety of processes. These can be split into the general categories of vat photopolymerization, powder bed fusion, material extrusion, material jetting, binder jetting, sheet lamination, and directed energy deposition. A type of vat photopolymerization, mask projection stereolithography, has

been used to successfully manufacture products with features under 10 μm in size [11], and it has been commercialized by multiple companies in Europe and the United States. Just like in other processes, a CAD file of a part is sliced into a high number of layers, but instead of building the layer one-dimensionally with lines of material, the entire layer is projected on a dynamic mask which selectively exposes the photopolymer to UV light [12]. This type of additive manufacturing is particularly suited to the micro scale because of the possibility of high resolution, and it has an added advantage of producing three-dimensional parts without support material that would be necessary in other processes [13].

2. SENSITIVITY ANALYSIS

Sensitivity analysis was performed on kinematically coupled, injection molded, polymer microfluidic modules. The analysis was used to determine which dimensions of the coupling features have the highest contribution to misalignment of the modules. Tolerance analysis by Monte Carlo simulation was previously done for these dimensions by You et al. (2015), but it only provides the distribution of variation of the assembly variables [2]. It does not give insight into which dimensions cause most of that variation.

Two critical terms that should be defined are component dimension and assembly variable. There does not seem to be a standard definition of them throughout the literature. Component dimensions refer to the manufactured dimensions of the modules. In this case, the component dimensions of interest are all dimensions of the kinematic coupling features which are the hemisphere-tipped posts and v-grooves. In the calculations discussed below, component dimensions are represented by independent variables that can be assigned random values within the range of that dimension's tolerance. Assembly variables refer to the dependent variables that represent the overall alignment of the modules. There are six assembly variables for the six degrees of freedom: rotation about the X, Y, and Z-axes (θ_X, θ_Y, θ_Z) and translation along the X, Y, and Z-axes (X, Y, Z). These variables are dependent on the values of the component dimensions.

The sensitivity analysis was done by multivariate error analysis and can be split into these general steps: creation of vector loops, solving for assembly variables, calculation of partial differentials, and creation of percent contribution charts. These general steps are shown in a flow chart in Figure 2.

2.1 Vector Loops

The first step in sensitivity analysis is to mathematically define the relationships between the component dimensions and the assembly variables. This is typically done by vector loops, where each vector represents at least one component dimension. There are six contact points in the kinematic coupling being analyzed, two for each post-v-groove connection. Each contact point has its own vector loop, shown in Figure 3, which contains four vectors: $P_{H_i}^{UM}$, $n_{CP_i}^{LM}$, $P_{CP_i}^{LM}$, T_{UM}^{LM}. The vectors are related by Equation 1 shown below [14].

$$T_{UM}^{LM} P_{H_i}^{UM} - P_{CP_i}^{LM} = \frac{D_{H_i}}{2} n_{CP_i}^{LM} \qquad \text{for } i = 1, \ldots, 6 \tag{1}$$

Where T_{UM}^{LM} is the transformation matrix from the origin of the lower module to the origin of the upper module, $P_{H_i}^{UM}$ is the vector from the origin of the upper module to the center of the hemisphere on the post, $P_{CP_i}^{LM}$ is the vector from the origin of the lower module to the contact point, $n_{CP_i}^{LM}$ is the normal vector from the surface of the v-groove to the center of the hemisphere, and D_{H_i} is the diameter of the hemisphere. The transformation matrix, T_{UM}^{LM}, contains the unknown assembly variables, so Equation 1 can be solved for the elements of $P_{CP_i}^{LM}$ to get the coordinates of contact point i in terms of the assembly variables (θ_X, θ_Y, θ_Z, X, Y, Z). This can be simplified by linearizing the transformation matrix. It could be expected that there may be concern over the accuracy of the calculations after such linearization, but it will be explained and shown in the next section that linear and nonlinear calculations produced the same results. The contact point equations can be substituted into Equation 2 to incorporate the vector representing the v-

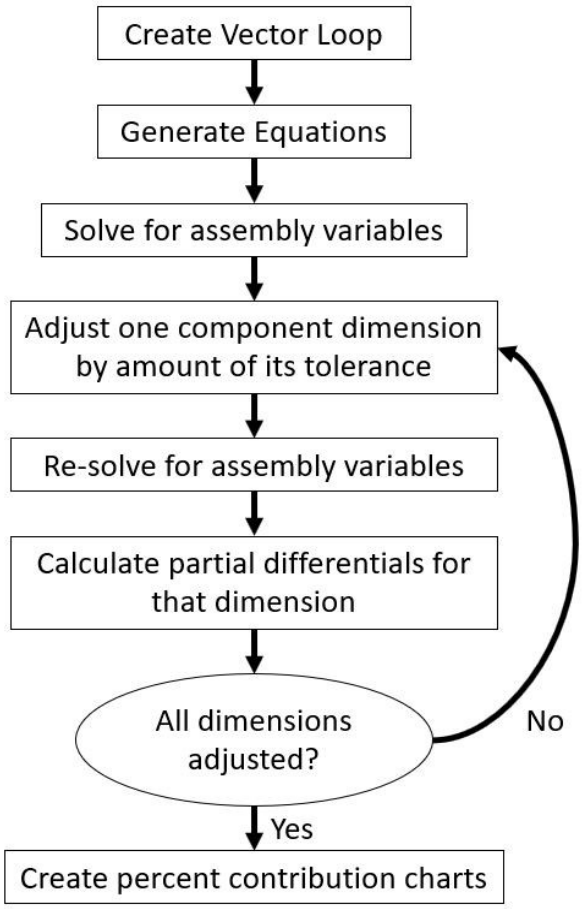

Figure 2. Multivariate Error Analysis Flow Chart.

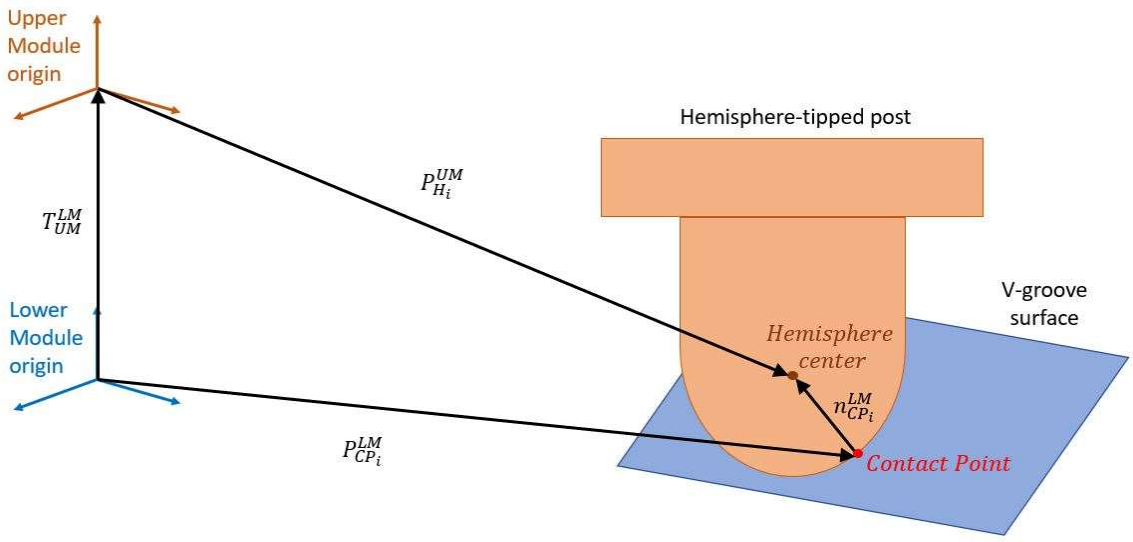

Figure 3. Vector Loop. The mathematical representation of a post-v-groove connection [2].

groove surface [14]. Doing this for all six contact points provides a system of six equations that can be solved for the assembly variables.

$$ {}^{x}n_{CP_i}^{LM}\left(x_{CP_i} - {}^{x}P_{S_i}^{LM}\right) + {}^{y}n_{CP_i}^{LM}\left(y_{CP_i} - {}^{y}P_{S_i}^{LM}\right) + {}^{z}n_{CP_i}^{LM}\left(z_{CP_i} - {}^{z}P_{S_i}^{LM}\right) = 0 $$
$$ \text{for } i = 1, \ldots, 6 \tag{2} $$

Where ${}^{x}n_{CP_i}^{LM}$, ${}^{y}n_{CP_i}^{LM}$, and ${}^{z}n_{CP_i}^{LM}$ are the elements of the normal vector from Equation 1, x_{CP_i}, y_{CP_i}, and z_{CP_i} are the coordinates of contact point i, and ${}^{x}P_{S_i}^{LM}$, ${}^{y}P_{S_i}^{LM}$, and ${}^{z}P_{S_i}^{LM}$ are the elements of a vector from the origin of the lower module to a point on the v-groove surface.

2.2 Solve for Assembly Variables

Once the system of six equations is found, solving for the assembly variables in MATLAB is simple. The coefficients of the assembly variables make a matrix (M), and the constants make a vector (V). The unknown values are then returned by the function *linsolve(M, V)*. However, to calculate the assembly variables iteratively, a program must be written to calculate the coefficients and constants directly from the component dimensions. This program is shown in Appendix D. It enables Monte Carlo simulations by setting the component dimensions to normally distributed random values with the tolerance equal to three standard deviations. The dimension mean and tolerance values used were measured from injection molded microfluidic modules by You (2008) and are shown in Table 1. Monte Carlo simulations were run using linear and nonlinear calculations with 10,000 iterations. The variation distributions, shown in Appendix A, for the assembly variables are very similar, and the mean and standard deviations are within 1 micron.

Table 1. Component Dimensions. From injection molded kinematic coupling features [3].

Dimension	Nominal Value	Measured Value
Post Radial Distance	16 mm	15.908 ± 0.003 mm
Post Radial Angle	0.00°	0.00 ± 0.01°
Post Nonplanarity	0 μm	-3 ± 8 μm
Post Height	925 μm	932 ± 15 μm
Post Base Height	100 μm	103 ± 6 μm
Post Radius	500 μm	485 ± 8 μm
Post Angle about X-axis	0.0°	-1.4 ± 0.4°
Post Angle about Y-axis	0.0°	0.0 ± 0.4°
Groove Radial Distance	16 mm	15.908 ± 0.003 mm
Groove Radial Angle	0.00°	0.00 ± 0.01°
Groove Nonplanarity	0 μm	-3 ± 8 μm
Groove Width	1890 μm	1877 ± 3 μm
Groove Angle	45.0°	44.9 ± 0.3°

2.3 Partial Differentials

The partial differentials are the sensitivities of the component dimensions to each of the assembly variables. Setting all the dimensions to their mean value and calculating the assembly variables provides the mean variation values. The partial differentials can be calculated by changing the value of one component dimension at a time, recalculating the assembly variables, and then dividing the change in the value of an assembly variable by the change in the component dimension. Each component dimension has six partial differentials, one for each assembly variable. The partial differentials for all the component dimensions form the Jacobian matrix $[J]$, with each dimension having its own column.

$$J = \begin{bmatrix} \frac{\Delta\theta_X}{\Delta d_1} & \cdots & \frac{\Delta\theta_X}{\Delta d_j} \\ \vdots & \ddots & \vdots \\ \frac{\Delta Z}{\Delta d_1} & \cdots & \frac{\Delta Z}{\Delta d_j} \end{bmatrix} \quad (3)$$

Where d_j is the jth component dimension. Considering first order terms in Taylor's series expansion, the variation of assembly variable θ_X is given by Equation 4 below. The other variables are given by the same equation, just with a different row of the Jacobian matrix [14].

$$\delta\theta_X = J_{11}\delta d_1 + J_{12}\delta d_2 + \cdots + J_{1j}\delta d_j \quad (4)$$

A single set of random component dimension values can be generated and used in both the MATLAB calculation and a manual calculation of Equation 4. Comparing the results of these verifies the accuracy of the sensitivities. This was done for all six assembly variables, and they all produced MATLAB and manual calculation values within 1 micron of each other. The consistent, near-exact match of these values is proof of the accuracy of the sensitivities.

2.4 Percent Contribution

After obtaining the sensitivities of the component dimensions in the Jacobian matrix, percent contribution charts can be made. They can be made with the worst-case method or statistical model. One of each kind was made for each assembly variable. They are shown in Appendix B. Statistical values are given by Equation 5 and worst case by Equation 6 [15].

$$PC_{ij} = \frac{(s_{ij}t_j)^2}{\sum_{j=1}^{39}(s_{ij}t_j)^2}\, x\, 100 \qquad \text{for } i = 1, \dots, 6 \tag{5}$$

$$PC_{ij} = \frac{|s_{ij}|t_j}{\sum_{j=1}^{39}|s_{ij}|t_j}\, x\, 100 \qquad \text{for } i = 1, \dots, 6 \tag{6}$$

Where PC_{ij} is the percent contribution of component dimension j to the variation of assembly variable i, s_{ij} is the sensitivity of dimension j to assembly variable i, and t_j is the tolerance of component dimension j.

Total contribution of each dimension can then be found to determine which ones are most important to alignment of the modules. Depending on the function of the modules, the assembly variables may all have equal weights, or some may be more important than others. For example, if a sample should be transferred from one module to the next by alignment of through-holes, perhaps the assembly variables that matter the most are rotation about z-axis (θ_Z), translation along x-axis (X), and translation along y-axis (Y). Each of these may be given weights of 25 percent, while translation along z-axis (Z) is set at 15, and rotation about x and y-axes are less important with 5 percent weights. Correction factors must then be calculated by dividing the given weight by 16.7 percent, which is the default weight because it is one of six assembly variables. Total contribution was calculated using these example weights, as well as with equal weights. It is given by Equation 7 below.

$$TC_j = \frac{\sum_{i=1}^{6} PC_{ij}F_i}{6} \qquad \text{for } j = 1,\ 2, \dots,\ 39 \tag{7}$$

Where TC_j is the total contribution of component dimension j, PC_{ij} is the percent contribution of component dimension j to the variation of assembly variable i, and F_i is the correction factor for assembly variable i.

It can be seen in Figure 4 that for the example assembly variable weights, the post angularity about the y-axis (Post Angle Y) is the highest contributing dimension, and the post height is the highest when using equal weights. Post and groove radial angle have significant contributions as well, but they also have very tight tolerances as can be seen in Table 1. To further tighten the tolerance on the post and groove radial angle dimensions would likely prove too costly. Post Angle Y and Post Height have relatively loose tolerances which would make improving them much more plausible. For these reasons, the best way to improve the alignment of injection molded, kinematically coupled microfluidic modules is to reduce the tolerances for Post Height and post angularity about the y-axis (Post Angle Y).

3. METHODOLOGY

The proposed solution to the misalignment caused by the hemisphere-tipped posts is to fabricate the posts separate from the main device modules. This approach eliminates the problem of demolding, and the posts could be manufactured with tighter tolerances. An alternative benefit of modularizing the posts is the potential for selective assembly. Some small inaccuracies on one post may be offset by equal and opposite inaccuracies on another. One promising method of fabrication of the posts is additive manufacturing. Micro-additive manufacturing has become possible with advances in processes such as projection stereolithography [12]. The major challenge to this proposed solution is the connection of the posts to the main microfluidic device module. 3D printing directly onto the module may alleviate this problem, though adhesion between the module surface and the printed post would then be an issue [16].

The original plan for this research was to directly test the proposed solution by fabricating hemisphere-tipped posts using additive manufacturing and experimenting with different methods of connection of the posts to a microfluidic module. The accuracy of each method would be determined by measuring the dimensions used in the sensitivity analysis explained in Chapter 2 and entering the measured values into the Monte Carlo simulation to compare the variation distributions for the assembly variables. However, unexpected restrictions on laboratory access and transactions with businesses due to the COVID-19 pandemic made completing these physical experiments impossible during the available time. Therefore, further simulations and calculations are used to both reinforce the sensitivity analysis and explore the originally proposed solution.

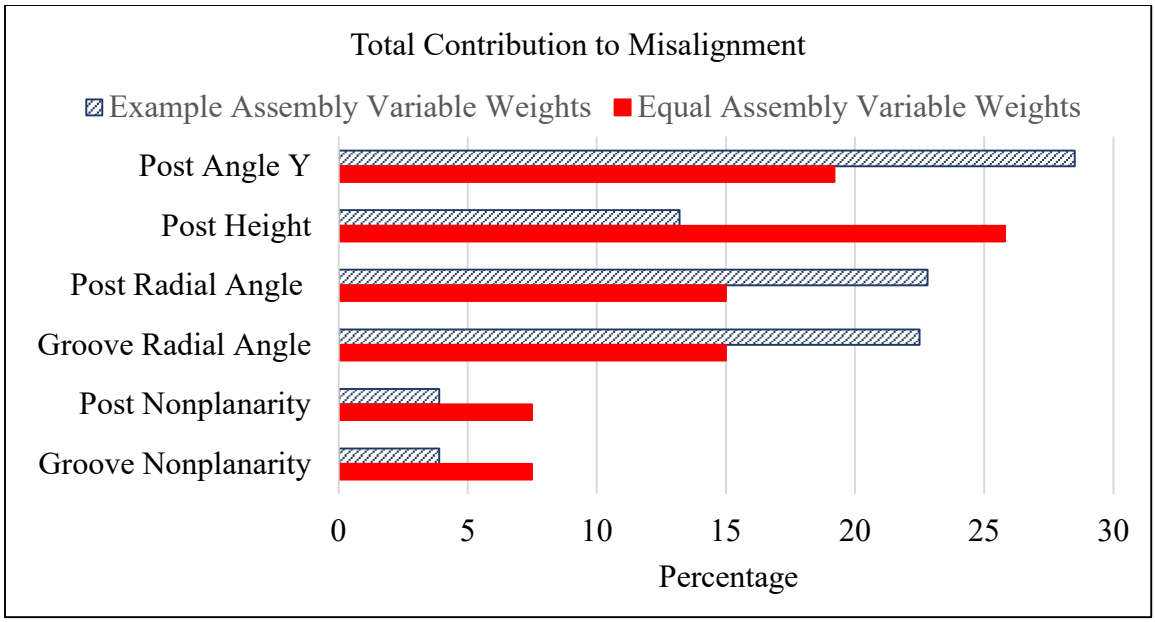

Figure 4. Total Contribution to Misalignment. Graph showing total contribution of component dimensions to assembly variable misalignment.

3.1 Covariance Calculation

The covariance matrix provides a method of calculating the variances of the assembly variables aside from the Monte Carlo simulation. It can also be used to find any correlation between variables. The covariance matrix for the assembly variables is given by Equation 8 [10].

$$[C_A] = [J][C_d][J]^T \tag{8}$$

Where $[C_A]$ is the assembly variable covariance matrix, $[C_d]$ is the component dimension covariance matrix, and $[J]$ is the Jacobian matrix. The component dimension covariance matrix is found by calculating the variances of the component dimensions and placing them in the diagonal elements. Since it is assumed that tolerances are equal to a three standard deviation range, it is a simple calculation to divide the bilateral tolerance by three and square the resulting value to produce the variance.

The off-diagonal elements are the covariances between the component dimensions and are assumed to be zero in this case. Dimensions that are formed using separate operations likely do have near zero correlation, but dimensions that are formed in the same or dependent operations will have at least some small correlation. For example, if a hole needs to be drilled to assist in locating a part on a fixture, the dimensions of features made while the locator hole is being used will be highly correlated to the dimensions of the hole [17]. In the case of the kinematic coupling component dimensions, there is likely some correlation between them when the modules are injection molded because many, if not all, of the features are being created in the same operation. To determine estimates of the covariance values between the component dimensions would require a significant number of injection molding experiments to collect data for regression analysis. That is beyond the scope of this research, but it could be a topic for future work.

There were slight differences between the variances calculated using the covariance matrix and the Monte Carlo simulation, but they are not significant enough to affect the results of this research. Both Rotation X and Rotation Y differed by an amount equal to 0.0055 and 0.0057 degrees, respectively, when converted to standard deviation. Translation Z differed by an amount equal to 1.1 microns when converted to standard deviation. The differences in the other variables were negligible. The values are shown in Table 2.

3.2 Functional Feature Misalignment

Determining the effect of variation in the assembly variables on the functional features of a device allows the estimation of desired assembly variable tolerances. The

Table 2. Covariance Matrix and Monte Carlo Simulation Comparison.

Assembly Variable	Standard Deviation Covariance Matrix	Standard Deviation Monte Carlo
Rotation X	0.0150°	0.0205°
Rotation Y	0.0147°	0.0204°
Rotation Z	0.0035°	0.0035°
Translation X	1.4 μm	1.4 μm
Translation Y	1.4 μm	1.4 μm
Translation Z	2.9 μm	4.0 μm

Monte Carlo simulation and the covariance matrix calculation both allow the calculation of achievable assembly variable tolerances depending on the component dimension tolerances. The component dimension tolerances can be altered to determine the change necessary to achieve the desired assembly variable tolerances as determined by the functional features. The Monte Carlo simulation was run using random, normally distributed component dimension values assuming the tolerances from Table 1 are equal to a three standard deviation (3σ) range. The resulting distributions are shown in Appendix A. The assembly variable tolerances were calculated using the same 3σ range and are shown in Table 3. The Monte Carlo simulation was chosen to calculate the tolerances because it employs a more robust method as compared to the covariance matrix calculation. However, the following calculations could be done using tolerances calculated from the covariance matrix, and the conclusions would not change.

3.2.1 Rotational Variation to Translational Misalignment

The example of a functional feature used in Section 2.4 was aligned through-holes for transfer of fluid between modules. Autodesk Inventor 2019 was used to simulate effects of variation in rotational assembly variables on aligned through-holes. This allows

Table 3. Assembly Variable Tolerances. Calculated by Monte Carlo simulation

Assembly Variable	Mean	Standard Deviation (σ)	Tolerance (3σ)
Rotation X	-0.0001°	0.0205°	± 0.0616°
Rotation Y	0.0001°	0.0204°	± 0.0612°
Rotation Z	0.0000°	0.0035°	± 0.0105°
Translation X	-0.01 μm	1.4 μm	± 4.1 μm
Translation Y	0.01 μm	1.4 μm	± 4.1 μm
Translation Z	299.4 μm	4.0 μm	± 12.0 μm

the conversion of rotational variation to translational misalignment. The results of the conversion can be added to the translational assembly variable tolerances to determine the worst-case functional feature misalignment.

An Inventor assembly of two module representations was created using rotational joints. The calculated tolerance for Rotation Z was ±0.0105 degrees. The Rotation Z assembly variable refers to the upper module of a two-module stack being rotated about the z-axis while the lower module remains fixed. This is illustrated in Figure 5. It was simulated by constraining the two stacked, aligned modules with a rotational joint so that the only degree of freedom is rotation about the z-axis. Holes were extruded on the y-axis every 5 mm from the center of the modules out to 30 mm. The difference in the x-axis coordinates of the centers of the holes in the stacked modules provided an estimate of misalignment. The upper module was rotated 0.0105 degrees, and the misalignment ranged from 0.87 μm at 5 mm from the center to 5.24 μm at 30 mm. The same misalignment value can also be estimated using a simple trigonometry identity, as shown in Equation 9.

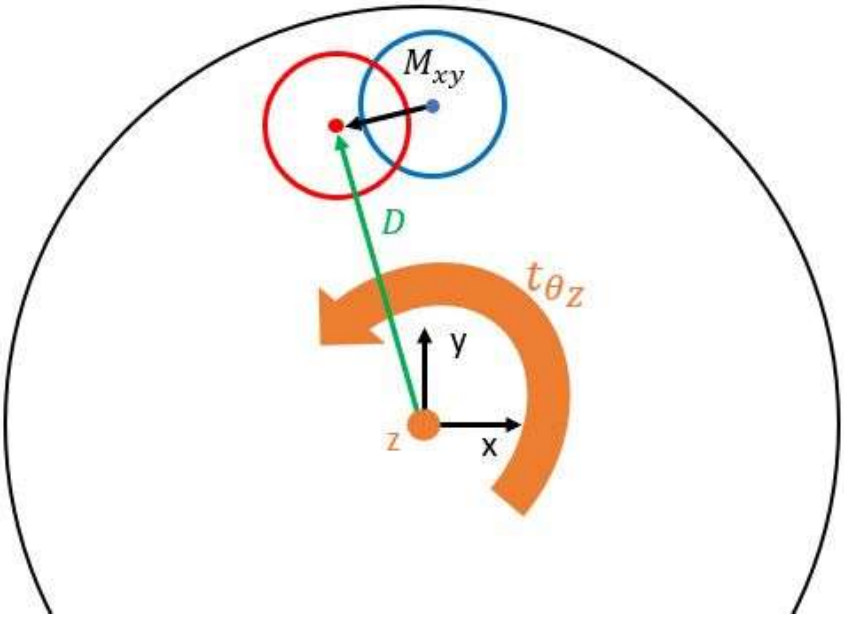

Figure 5. Functional Feature Misalignment Due to Rotation Z. Schematic illustrating Equation 9.

$$M_{xy} \cong D \tan(t_{\theta_Z}) \tag{9}$$

Where $\boldsymbol{M_{xy}}$ is functional feature misalignment in the x-y plane, D is the distance from the center of the module to the feature, and $\boldsymbol{t_{\theta_Z}}$ is the tolerance for Rotation Z.

The misalignment due to Rotation X and Y is in the z-axis direction and can be calculated using the same identity as shown in Equation 10.

$$M_z \cong D_y \tan(t_{\theta_X}) - D_x \tan(t_{\theta_Y}) \tag{10}$$

Where $\boldsymbol{M_z}$ is functional feature misalignment in the z-axis direction, $\boldsymbol{D_y}$ is the y-coordinate of the feature, $\boldsymbol{t_{\theta_X}}$ is the tolerance for Rotation X, $\boldsymbol{D_x}$ is the x-coordinate of the feature, and $\boldsymbol{t_{\theta_Y}}$ is the tolerance for Rotation Y. As expected, the misalignment due to rotational assembly variables increases with distance from the center of the modules. Using example coordinates for a through-hole allows the calculation of a worst-case misalignment scenario. At (-18, 18), the z-axis misalignment due to the upper limit of

Rotation X and Y tolerances is 38.58 μm. Added to the upper limit of the Translation Z assembly variable tolerance, the worst-case z-direction variation is 50.59 μm.

The misalignment due to Rotation Z can be parsed into x- and y-direction or simplified as an x-y plane translational value. It is logical in this case to simplify it to a single x-y plane value because the hole is circular and located 45 degrees between the axes. Therefore, the separate x- and y-axis misalignment values will be the same, and they are not important as compared to the hypotenuse between them. However, it would be beneficial to parse the misalignment into x- and y-values in circumstances when the radial angle of the feature between the axes is anything other than 0 or 45 degrees. In such a case, it is easier to add the parsed x- and y-values to the Translation X and Y assembly variable values, then take the hypotenuse to determine the total x-y plane misalignment.

In the present example, the coordinates of the through-hole are (-18, 18), so it is located at 45 degrees between the axes. Therefore, the single x-y plane variation value due to Rotation Z can be added to the hypotenuse of Translation X and Y assembly variable values because the angles align. The x-y plane value due to Rotation Z converts to 4.67 μm. The hypotenuse of Translation X and Y assembly variable tolerances is 5.83 μm. Added to the x-y plane value, the total worst-case x-y plane variation is 10.5 μm.

3.2.2 Target Precision

The necessary component dimension tolerances will ultimately depend on the functional feature tolerances. If known, the process can be worked backward to determine the needed decrease in tolerance of component dimensions, most notably Post Height and

Post Angle Y since these were previously identified as having the highest total contribution to variation in assembly variables. In this manner, a target precision is identified for 3D printed hemisphere-tipped posts. It must first be verified that it is possible for posts to be consistently replicated by additive manufacturing while meeting the target precision. If it is determined to be possible, the next and most difficult challenge is developing a method of connection of the posts to a module. The method must be easily repeatable and passively provide alignment with the same high standard of precision. These are the topics covered in Chapter 4.

Since functional feature tolerances are unknown in this case, component dimensions Post Height and Post Angle Y were iteratively decreased to produce the smallest possible assembly variable tolerances. A point of diminishing returns was found at about ± 3 μm for Post Height and ± 0.05° for Post Angle Y. This is shown in the graphs in Figure 6 and Appendix C. Disregarding feasibility of the post tolerances, the maximum decrease in assembly variables tolerances achievable by only tightening Post Height and Post Angle Y tolerances are 30.2 percent for Rotation X, 29.7 percent for Rotation Y, 21.9 percent for Rotation Z, 22.5 percent for Translation X, 21.5 percent for Translation Y, and 28.6 percent for Translation Z.

By grouping the assembly variables by the type of functional feature misalignment they cause, the reduction in misalignment can be estimated by averaging the assembly variable reductions of the two groups. Rotation X, Rotation Y, and Translation Z are responsible for z-direction misalignment, and the average of their reductions is 29.5 percent. Rotation Z, Translation X, and Translation Y are responsible means that by only adjusting Post Height and Post Angle Y dimension tolerances, the

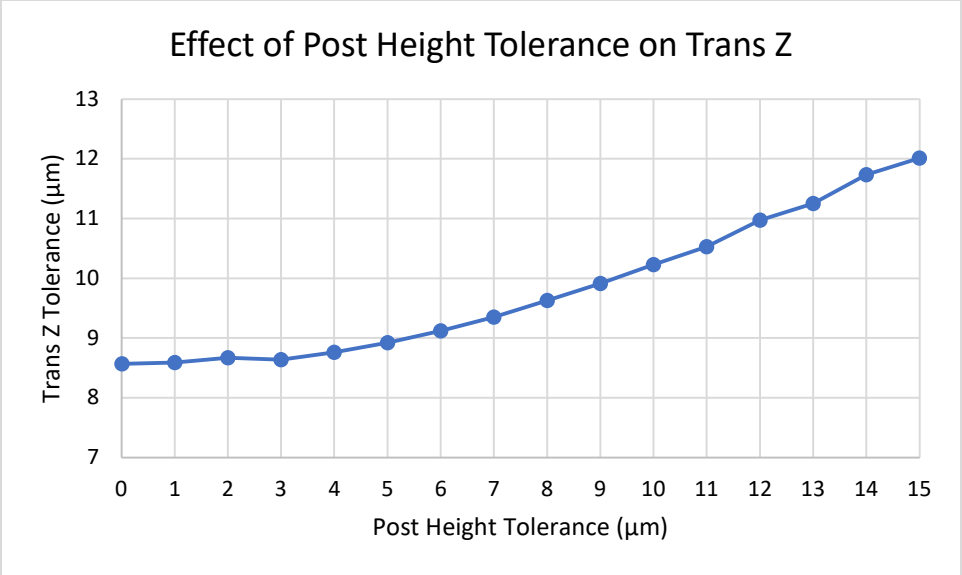

Figure 6. Effect of Post Height Tolerance on Translation Z. This graph shows the point of diminishing returns in decreasing the tolerance of the Post Height component dimension.

lowest possible worst-case functional feature misalignment is 35.7 µm for z-direction and 8.2 µm for x-y plane. This estimation has been checked by Equations 9 and 10.

The focus on Post Height and Post Angle Y is due to them being the highest contributing dimensions as determined in the sensitivity analysis. However, there are other dimensions that could achieve a decrease in tolerance by modularizing the hemisphere-tipped posts. These include Post Base Height, Post Radius, and Post Angle X. It is unclear whether Post Nonplanarity could be tightened by the modularization, but it shows the most promise by far of the remaining dimensions for further decreasing the assembly variable tolerances. This fact is shown by its 7.5 percent total contribution in Figure 4, making it the fifth highest contributing component dimension.

When the tolerance of Post Nonplanarity is also decreased in combination with Post Height and Post Angle Y, the maximum reduction in worst-case functional feature misalignment is 41.1 percent in the z-direction. As can be seen in the percent contribution

charts in Appendix B, Post Nonplanarity has essentially zero effect on Rotation Z, Translation X, or Translation Y, which are the assembly variables responsible for x-y plane functional feature misalignment. This is logical since it is a z-direction dimension.

If the tolerances of all the other post dimensions mentioned above, excluding Post Nonplanarity, are decreased along with Post Height and Post Angle Y, the maximum reduction in worst-case z-direction misalignment is 37.8 percent. By comparison, the combination of Post Base Height, Post Radius, and Post Angle X has less of an effect than Post Nonplanarity alone. These dimensions, like Post Nonplanarity, also have no effect on x-y plane misalignment. If Post Nonplanarity is not affected by the modularization of the posts, 37.8 percent is the maximum reduction in worst-case z-direction misalignment possible by the solution presented in this research. The value with such reduction would be 31.47 μm.

If Post Nonplanarity is included in the dimensions affected by modularization of the posts, the maximum possible reduction achieved by decreasing all aforementioned post dimension tolerances is 51.2 percent. This would bring the value of worst-case z-direction functional feature misalignment down to 24.69 μm. The worst-case x-y plane misalignment is still 8.2 μm. The proximity to these lowest possible values that is actually achievable remains to be determined, partially by examination of 3D printed hemisphere-tipped posts in Chapter 4, and partially by future work in combining the posts with a module.

While all previous discussion has concerned the reduction of post dimension tolerances, it is informative and could prove useful to also consider reduction of groove dimension tolerances. Disregarding ability to achieve tightened component dimension

Table 4. Assembly Variable Tolerances After Reduction of Post Dimension Tolerances. Calculated by Monte Carlo simulation after decreasing tolerances for Post Height, Post Angle Y, Post Angle X, Post Base Height, Post Radius, and Post Nonplanarity.

Assembly Variable	Tolerance (3σ) before Modularization	Smallest Possible Tolerance (3σ) after Modularization
Rotation X	± 0.0616°	± 0.0297°
Rotation Y	± 0.0612°	± 0.0299°
Rotation Z	± 0.0105°	± 0.0082°
Translation X	± 4.1 μm	± 3.2 μm
Translation Y	± 4.1 μm	± 3.2 μm
Translation Z	± 12.0 μm	± 5.9 μm

tolerances, the smallest possible assembly variables tolerances when reducing both post and groove dimension tolerances are shown in Table 5. The tolerances of the assembly variables responsible for functional feature z-direction misalignment, Rotation X, Rotation Y, and Translation Z, are reduced to insignificance. Therefore, using the same example as above of a feature located at (-18, 18), the lowest possible worst-case z-direction misalignment would be 0.02 μm.

However, the tolerances of the assembly variables responsible for x-y plane misalignment, Rotation Z, Translation X, and Translation Y, see no change at all compared to when only post dimension tolerances are reduced. This is logical and offers the conclusion that the only way to further reduce x-y plane misalignment is to reduce the tolerances of Post Radial Angle or Groove Radial Angle. There is no way to do this by the modularization proposed in this research. It would be difficult to do anyway since, despite their high total contribution of 15 percent as seen in Figure 4, their tolerances are already quite low at ±0.01 degrees.

Table 5. Assembly Variable Tolerances After Reduction of Post and Groove Dimension Tolerances. Calculated by Monte Carlo simulation after decreasing tolerances for Post Height, Post Angle Y, Post Angle X, Post Base Height, Post Radius, Post Nonplanarity, Groove Nonplanarity, Groove Width, and Groove Angle.

Assembly Variable	Tolerance (3σ) before Modularization	Smallest Possible Tolerance (3σ) after Modularization
Rotation X	± 0.0616°	± 0.0001°
Rotation Y	± 0.0612°	± 0.0001°
Rotation Z	± 0.0105°	± 0.0082°
Translation X	± 4.1 μm	± 3.2 μm
Translation Y	± 4.1 μm	± 3.2 μm
Translation Z	± 12.0 μm	± 0.02 μm

Since it is theoretically possible to reduce functional feature z-direction misalignment to insignificance when groove dimension tolerances are reduced in addition to post dimension tolerances, it is useful to estimate the reduction in misalignment that is actually possible to achieve. Without analyzing samples of 3D printed posts or grooves or experimenting with methods of connection to a module, a very rough estimate of achievable component dimension tolerances can be given by the resolution of the 3D printer used to print the parts. The resolution of the microArch™ S130 projection micro-stereolithography (PμSL) machine developed by Boston Micro Fabrication is 2 μm. Therefore, setting the translational component dimension tolerances to 2 μm will give a rough estimate of the assembly variable tolerances that could potentially be achieved. However, the 3D printer resolution does not assist with estimation of angular tolerances, so the only way to give them a realistic value is to set them equal to the measured tolerance of another component dimension. As mentioned above, the tolerance of Post Radial Angle is ±0.01 degrees, so that will be the tolerance of the other angular

component dimensions in the estimate of potentially achievable assembly variable tolerances.

The result of the simulation is shown in Table 6. Due to the point of diminishing returns, functional feature x-y plane misalignment remains unchanged. However, the reduction in worst-case z-direction misalignment is 79.9 percent, leading to a value of 10.17 μm. That is 58.8 percent lower than the maximum possible reduction by reducing post dimension tolerances alone.

4. HEMISPHERE-TIPPED POST DESIGNS AND EXAMPLES

4.1 3D Printed Hemisphere-Tipped Posts

A set of three hemisphere-tipped posts were additively manufactured by Boston Micro Fabrication (BMF) with their microArch™ S130 projection micro-stereolithography (PμSL) machine. The material used is proprietary and referred to as HTL, but it has mechanical properties similar to PMMA as shown in Table 7. As previously mentioned, the machine used has a resolution of 2 μm. The build volume in the smallest mode is 3.84 x 2.16 x 10 mm, which would eliminate the possibility of the combined ring post connection method. The largest mode is 50 x 50 x 10 mm, but presumably may have lower resolution.

The hemisphere-tipped posts (Figure 7) were measured with a Nikon Measuring Microscope MM-800 with a Lumenera Infinity 1 Microscopy Camera and a Heidenhain Quadra-Chek digital readout. The Post Radius was measured using a three-point circle calculation in the Infinity Analyze software as shown in Figure 8. Post Height and Post Base Height were measured by the z-axis discrepancy between focus on the respective surfaces at 200x magnification. Measurements of these linear dimensions were also attempted from a side view, but the accuracy is in question since the angle the post was resting at could not be verified. Post Angle Y and Post Angle X could not be measured, but the range of values of the dimensions that could be measured provide insight into the capabilities of micro-additive manufacturing.

The measured mean and tolerance values are shown in Table 7, but the largest tolerance is ±1.3 μm. That is the tolerance for Post Height, which is a 91% reduction

Table 6. Assembly Variable Tolerances Considering 3D Printer Resolution. Calculated by Monte Carlo simulation after setting component dimension tolerances equal to resolution of micro-3D printer.

Assembly Variable	Tolerance (3σ) before Modularization	Smallest Possible Tolerance (3σ) after Modularization
Rotation X	± 0.0616°	± 0.0122°
Rotation Y	± 0.0612°	± 0.0125°
Rotation Z	± 0.0105°	± 0.0082°
Translation X	± 4.1 μm	± 3.2 μm
Translation Y	± 4.1 μm	± 3.2 μm
Translation Z	± 12.0 μm	± 2.4 μm

Table 7. Comparison of HTL and PMMA Mechanical Properties. [18], [19], [20]

Property	BMF HTL	PMMA
Young's modulus (GPa)	4.2	2.9
Tensile strength (MPa)	79.3	75
Elongation (%)	2.23	4.5
Bending strength (MPa)	120.6	110
Hardness (Rockwell)	90 Shore D	90
Glass temperature (°C)	172	105

from the measured tolerance of the injection molded module shown in Table 1. It is also noteworthy that not only is the precision much better, but the accuracy is substantially improved as well, with the mean values being closer to the nominal values. While only three posts were measured, this is a good indicator that the tolerance of 2 μm used in the last simulation of the previous section is within the capabilities of additive manufacturing technology.

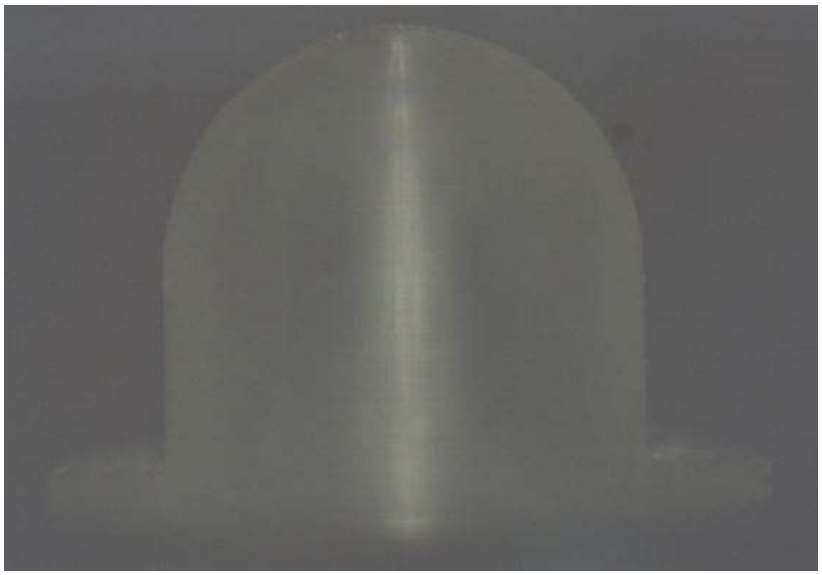

Figure 7. Side View of 3D Printed Hemisphere-tipped Post. 50x magnification side view of post printed by PμSL by Boston Micro Fabrication.

Since the additive manufacturing capabilities are likely not an issue, the only remaining challenge to improving alignment by modularization of the posts is the connection of the posts to a separate module. Besides the problem of post alignment and human error, the adhesion between the post and module must be experimented with as well. The additive manufacturing material used for the posts measured is a proprietary material, and that will likely be the case with many additive manufacturing companies. Therefore, the bond between such a material and an injection molded module of PMMA or PC can only be assessed by experimentation, and the results could not easily be generalized to multiple materials.

4.2 Post-Module Connection Designs

The precise and repeatable connection of the 3D printed hemisphere-tipped posts to an injection molded module is the most challenging part of the proposed solution. The ideal method of connection would provide passive alignment with micro-scale precision

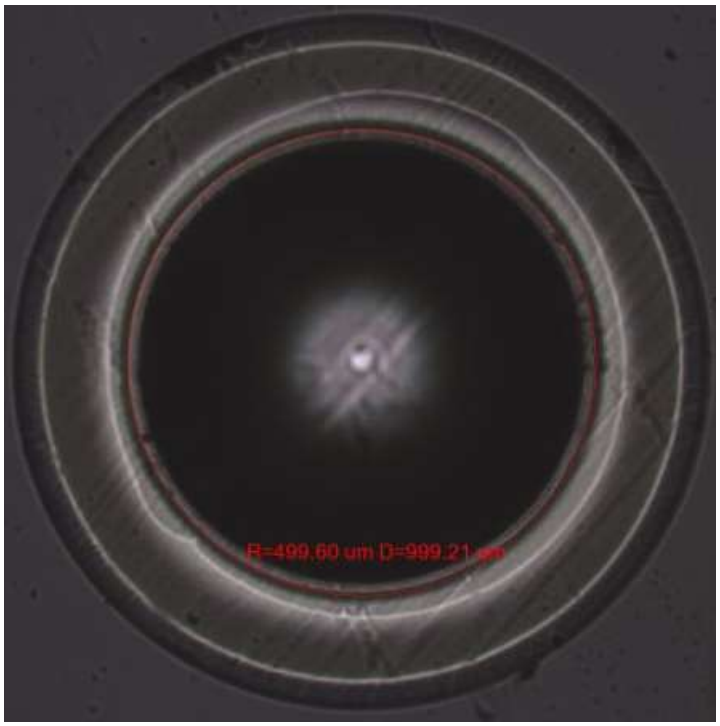

Figure 8. Measurement of Post Radius. Infinity Analyze measurement at 50x magnification of the Post Radius dimension of a post printed by PμSL by Boston Micro Fabrication.

Table 8. Measured Dimensions of 3D Printed Posts. Mean and tolerances of post dimensions of three hemisphere-tipped posts additively manufactured by Boston Micro Fabrication using projection micro-stereolithography.

Component Dimension	Nominal (μm)	Mean (μm)	Measured Tolerance (μm)
Post Height	900	902.9	± 1.3
Post Base Height	100	105.0	± 0.6
Post Radius	500	499.3	± 0.5

using only macro-scale instruments to perform it. It should be simple and foolproof so that it does not greatly increase cost of production.

4.2.1 Individual Post Connection Method

One of the potential methods of connection involves each post on a module being connected individually using male-female connectors. The male connector is on the post,

on the opposite surface of the post base from the hemisphere-tipped post itself. Experiments are necessary to prove viable dimensions, but initial dimensions and general design can be estimated. The male connector has a base diameter of 1 mm to support the actual post during additive manufacturing. The connector is 0.2 mm in length and tapers down to a 0.85 mm diameter to provide ease of assembly and draft angle for the injection molded female connector. The post base diameter is reduced from 1.5 mm to 1.2 mm and the interface between the base of the male connector and the post base surface is filleted. The fillet eliminates an otherwise sharp inside corner on the injection molding insert for formation of the female connector. Sharp inside corners are problematic to fill completely in injection molding [8]. The post base is retained only to aid in assembly. After experiments it could be deemed unnecessary. This individual post design is shown in the CAD model in Figure 9.

The injection molded module contains the female connector. It is illustrated in Figure 10. Bonding options for this method include external adhesive, interference fit, thermal bonding, or some combination of these. A snap-interference fit, where the largest diameter of the male connector on a post is located at the end of the connector and is larger than the diameter of the middle portion of the female connector on the module, could prove to be secure and accurate without external adhesive or other bonding techniques, but the geometry required of such a female connector on the module would likely be difficult or impossible to create by injection molding.

This individual method of connection could also provide the benefit of selective assembly. The connector would have an asymmetrical shape, instead of a cylindrical shape, to restrict assembly to unambiguity. The post angle dimensions could then be

Figure 9. Individual Post Design. Two-dimensional and three-dimensional views of individual post design with male connector.

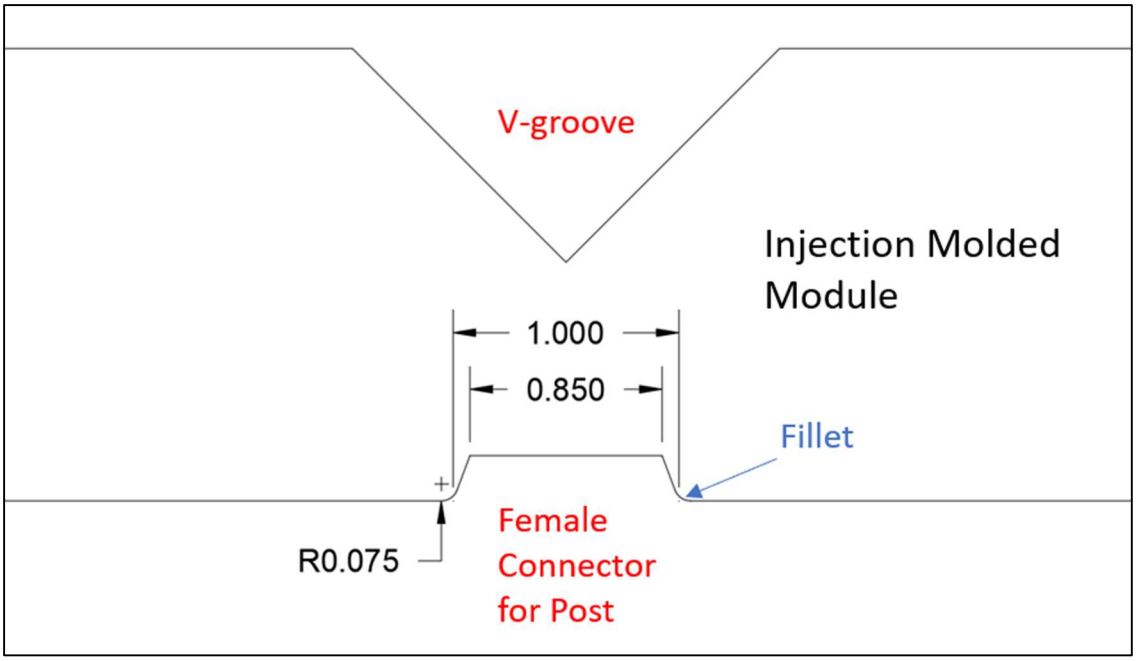

Figure 10. Female Connector for Individual Post. Drawing of module section showing v-groove and female connector for the individual post design.

measured in reference to the module coordinate system, and three posts with angle variations that cancel each other out could be selected for a module. However,

implementing such a procedure would require 100 percent inspection of the posts which could prove costly for mass manufacturing.

4.2.2 Combined Post Ring Connection Method

Another potential method of connection combines a set of three posts into one part. The posts would be connected to each other by a thin ring, which would also contain an alignment feature to make assembly unambiguous. The benefit of this type of connection method is ease and speed of assembly. Since the nominal Post Radial Distance from the origin of a module is 16 mm, the diameter of the ring would be roughly 32 mm, making handling of the part much less tedious and more macro-scale oriented.

The downside of the ring method is that holding the necessary micro-scale tolerances on a part with an overall macro-scale size is a significant challenge. Some micro 3D printers have too small of a build volume to print a part that size, and ones that do not may have too low of resolution. Combining the posts into a single part also eliminates the possibility of selective assembly, and the ring may restrict the number and location of functional features such as microchannels. This connection method has several limitations, but if they could be overcome there is no doubt it would enable faster and more efficient assembly than the individual post connection method described in the previous section. A model of the combined post ring connection method is shown in Figure 11.

4.2.3 Two-Part Post Connection Method

The final potential connection method discussed in this research involves a second part besides the post itself. It is shown in Figure 12. It is unique from the other

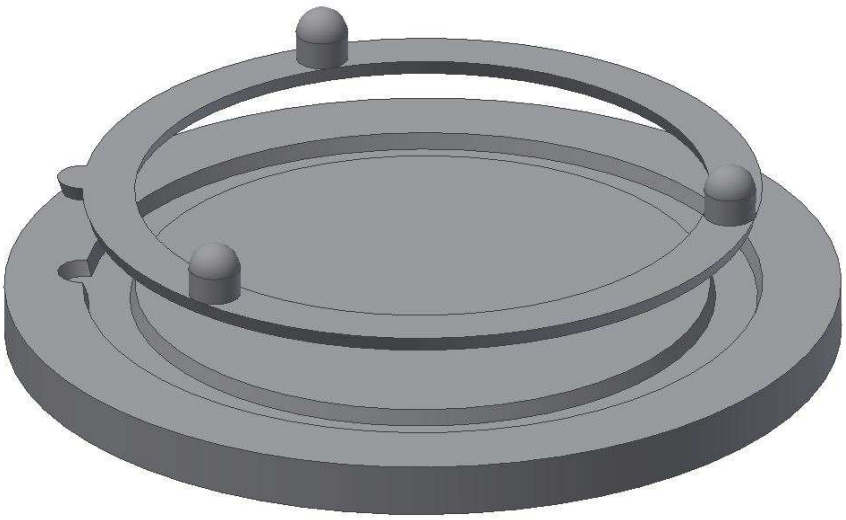

Figure 11. Combined Post Ring Connection Method. Three-dimensional model of exaggerated post ring connection method.

two designs in that it also involves 3D printing the groove. This produces the major benefit of decreasing the component dimension tolerances for some of the groove dimensions in addition to the post dimensions, further reducing the functional feature z-direction misalignment as explained in Section 3.2.2. In addition, the parts must have a larger diameter than the individual post design which could make them slightly easier to handle and assemble without special instrumentation. Selective assembly would also be an option for this design. The main downside of this design is that more parts provides more opportunity for something to fail or cause misalignment.

The design of the post is roughly the same concept as the individual post connection method shown in Figure 9, but the angled male connector has a larger diameter and a length equal to half the thickness of the module. The groove is on the end of a second male connector that is also the length of half the thickness of the module. The female connector on the module is a through-hole with a draft angle to match the angle on the male connectors. The groove part and the post part are stacked, flat ends mating,

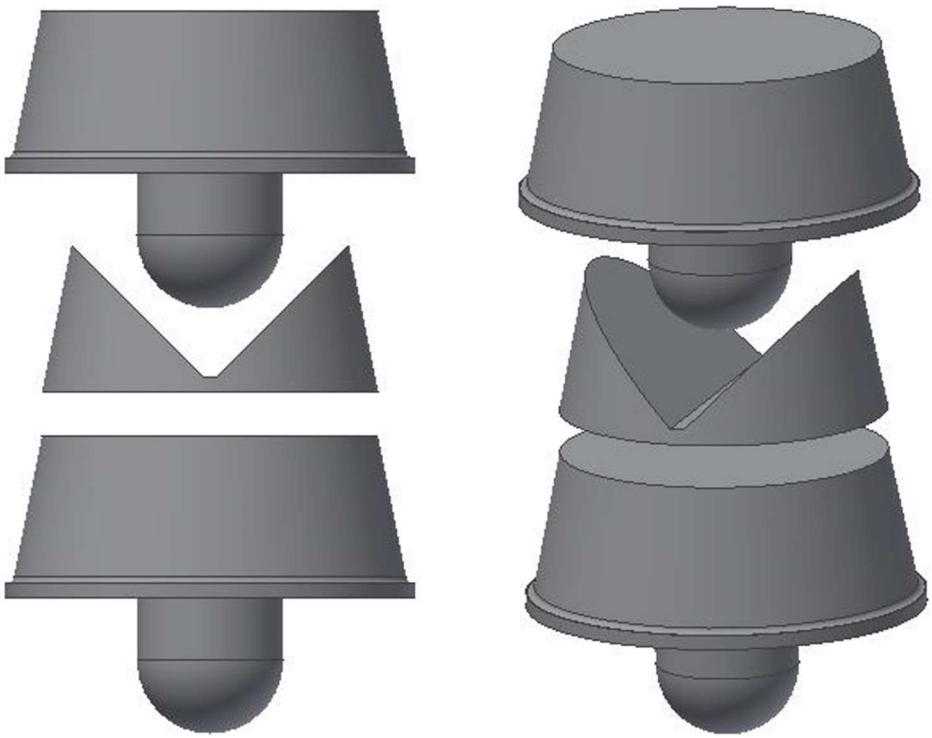

Figure 12. Two-Part Post Connection Method. Two-dimensional and three-dimensional views of the two-part post connection design, with an extra post part to show stacking of second module.

inside of the through-hole so that the angle of the side of the groove part is continued by the post part. Both the through-hole and the male connectors could have unique shapes to facilitate unambiguous assembly, though it may be unnecessary and only decrease efficiency of assembly.

5. CONCLUSIONS AND FUTURE WORK

Kinematic couplings are a method of achieving exact constraint between stacked microfluidic device modules. The coupling used in this research is a set of three hemisphere-tipped posts contacting a set of three v-grooves. It was determined through sensitivity analysis that the height and angularity of the posts about the y-axis are the dimensions with the highest contribution to misalignment of the modules. It was proposed that fabricating the posts separately from the module and then connecting them will enable tighter tolerances for these dimensions, and therefore improve the overall alignment.

Misalignment of functional features such as through-holes is the ultimate constraint for any device, and the tolerances of such misalignment determine the necessary assembly variable tolerances. Functional feature misalignment was grouped into horizontal and vertical misalignment, or x-y plane and z-direction misalignment, respectively, and related to the appropriate assembly variables by equations. Since the Monte Carlo simulation outputs the variation in assembly variables, the functional feature misalignment can be found for any change in the component dimensions. Therefore, if functional feature tolerances are known, component dimensions tolerances can be reduced until they are met.

The worst-case functional feature misalignment without reduction in component dimension tolerances is 50.59 μm in the z-direction and 10.5 μm in the x-y plane. The minimum worst-case misalignment achievable by reducing only the post dimension tolerances is 24.69 μm in the z-direction and 8.2 μm in the x-y plane, a 51.2 and 22 percent reduction, respectively. When groove dimension tolerances are also reduced, x-y

plane misalignment remains constant, but minimum z-direction misalignment drops to 10.17 μm, a 79.9 percent reduction, using a realistic component dimension tolerance of 2 μm.

Additive manufacturing is a potential method of post fabrication, specifically material jetting and stereolithography. Hemisphere-tipped posts were additively manufactured by projection micro-stereolithography by Boston Micro Fabrication. The measured post dimensions produced a maximum tolerance of ±1.3 μm. This is a good indicator of the capability of additive manufacturing technology to achieve the necessary precision.

Three different post connection designs were proposed as options for connecting the modularized posts to separate modules. Experimentation with these designs is needed to determine if precision can be maintained. Other future work includes determining the covariances between component dimensions by regression analysis on data collected through injection molding experiments. This work provides guidelines for systematically improving alignment of injection molded polymer kinematic couplings and explores the possibility of doing so through employment of additive manufacturing. Improving the alignment of kinematically coupled microfluidic modules by modularizing the coupling features can contribute to the realization of mass production of precisely aligned polymer microfluidic devices.

APPENDIX SECTION

APPENDIX A: LINEAR AND NONLINEAR COMPARISON

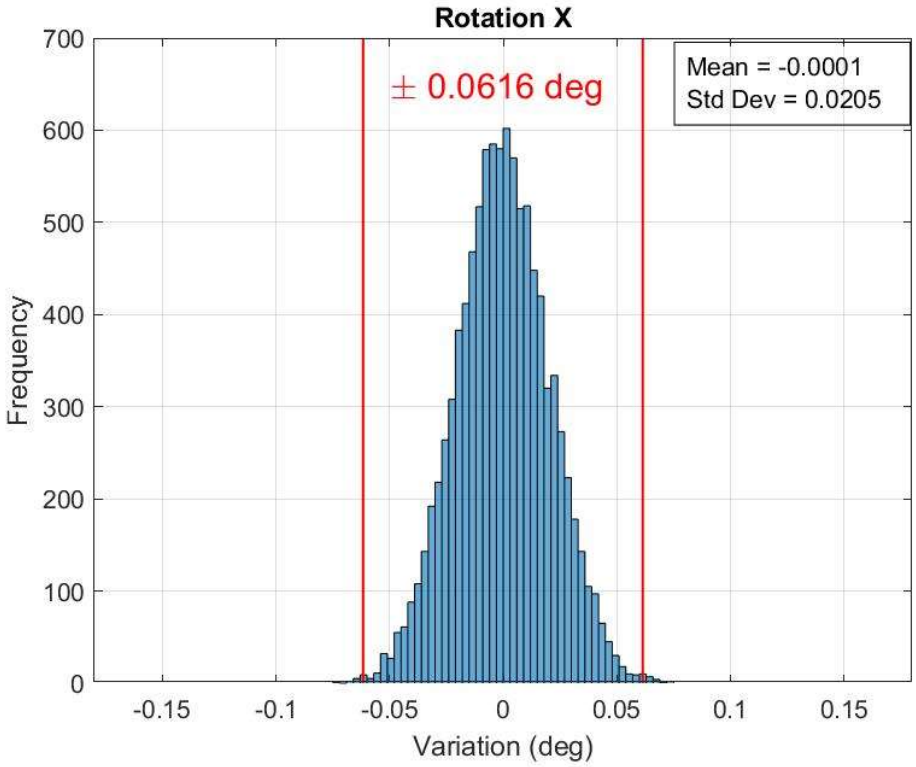

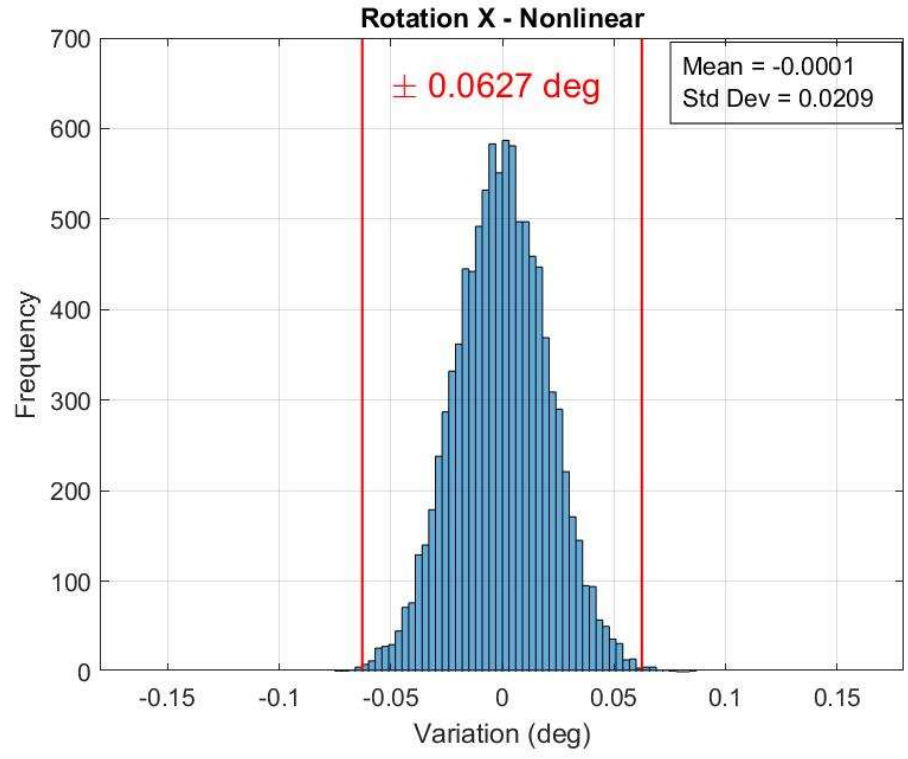

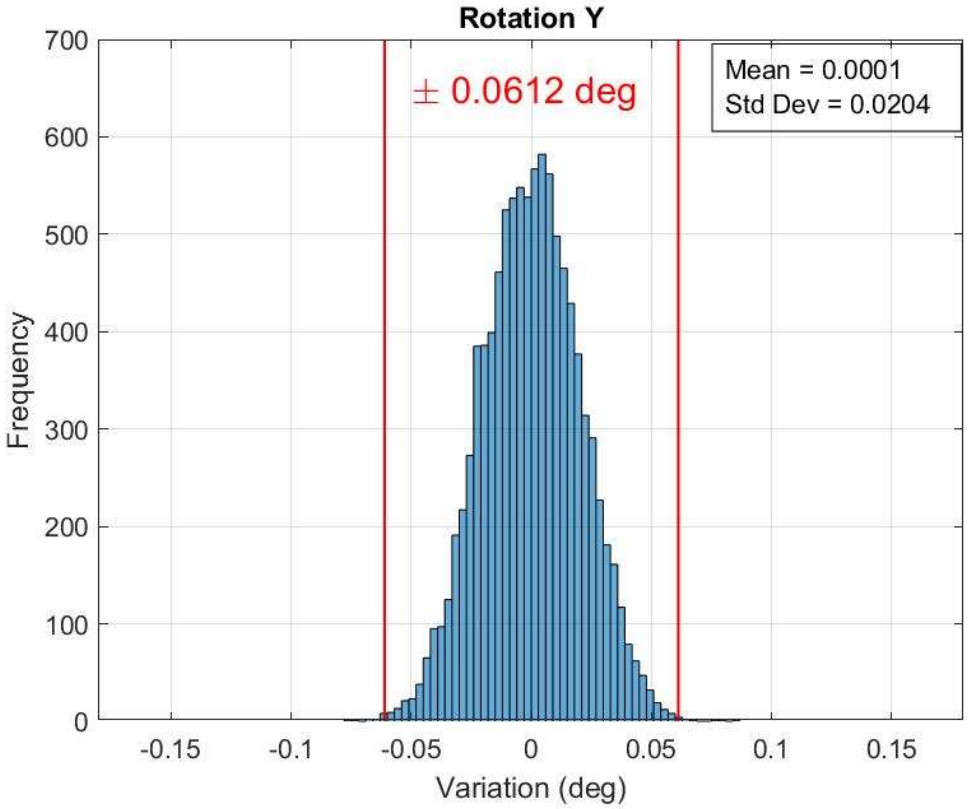
Rotation Y
± 0.0612 deg
Mean = 0.0001
Std Dev = 0.0204
Frequency
Variation (deg)
0
100
200
300
400
500
600
700
-0.15
-0.1
-0.05
0
0.05
0.1
0.15

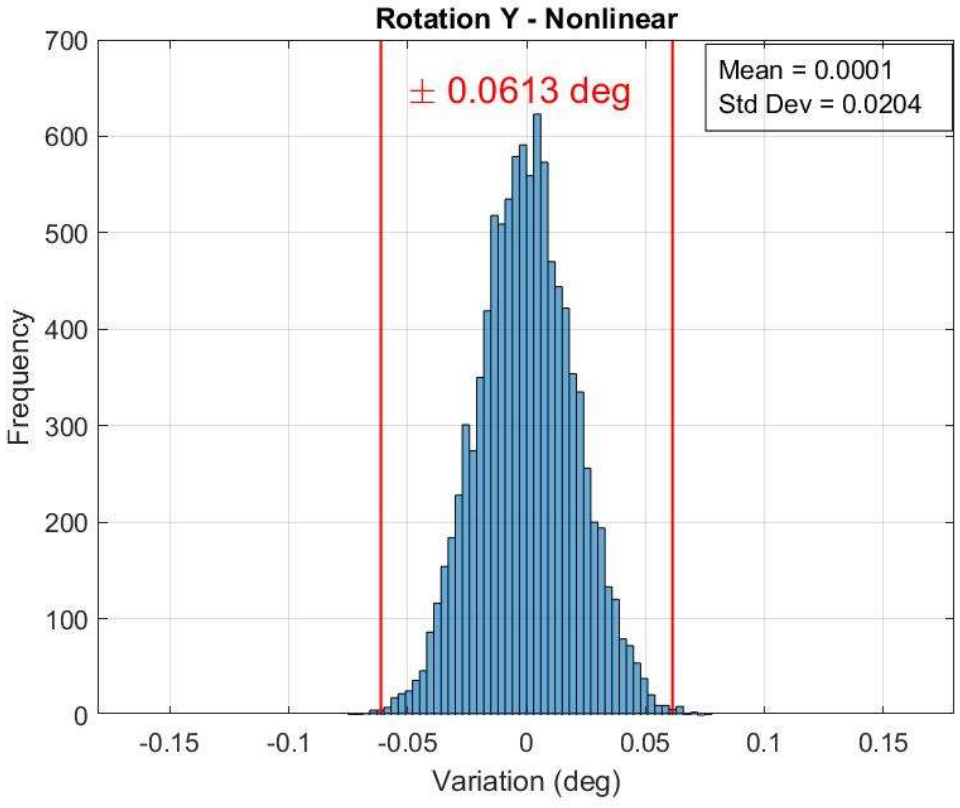
Rotation Y - Nonlinear
± 0.0613 deg
Mean = 0.0001
Std Dev = 0.0204
Frequency
Variation (deg)
0
100
200
300
400
500
600
700
-0.15
-0.1
-0.05
0
0.05
0.1
0.15

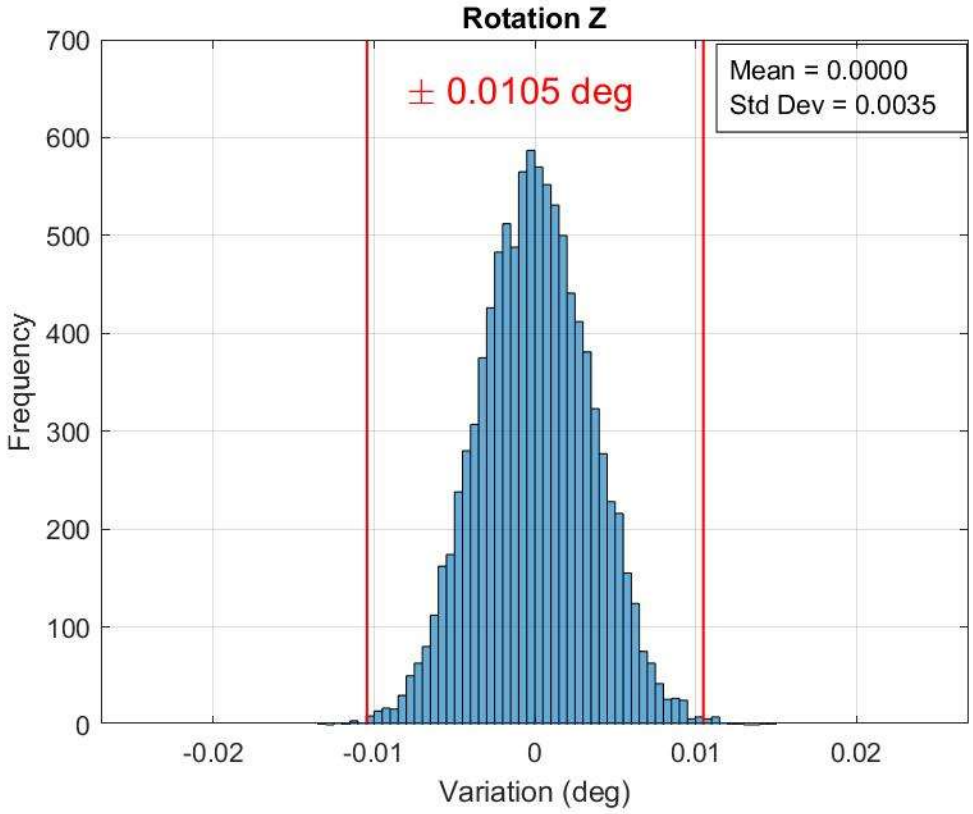
Rotation Z
± 0.0105 deg
Mean = 0.0000
Std Dev = 0.0035
Frequency
Variation (deg)
700
600
500
400
300
200
100
0
-0.02
-0.01
0
0.01
0.02

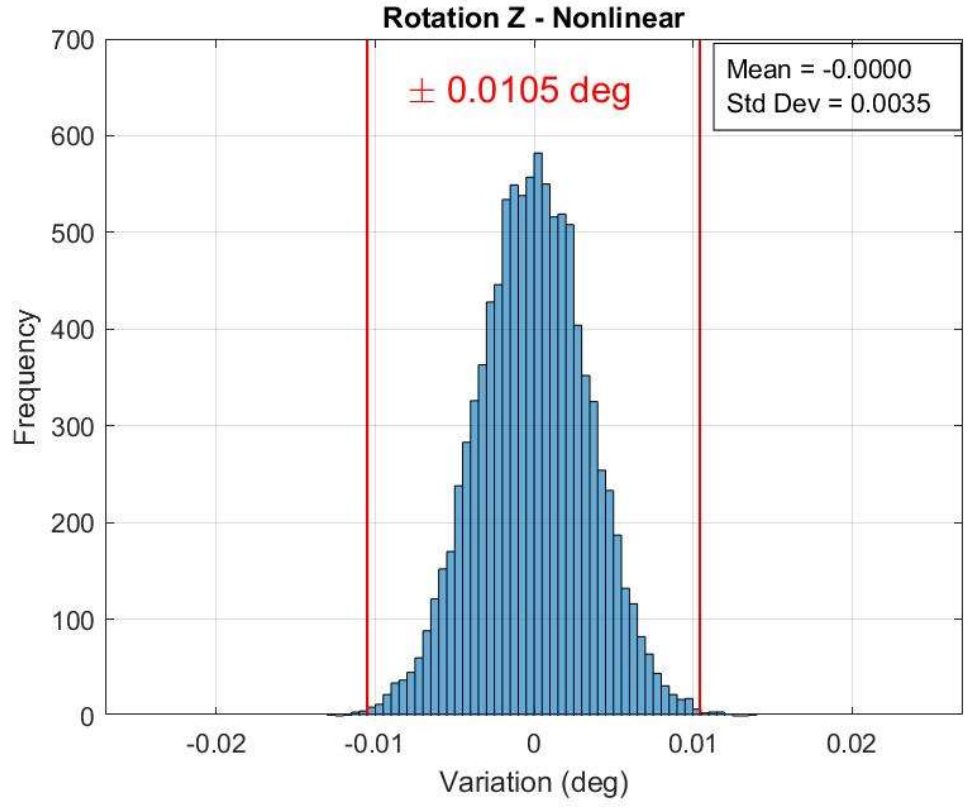
Rotation Z - Nonlinear
± 0.0105 deg
Mean = -0.0000
Std Dev = 0.0035
Frequency
Variation (deg)
700
600
500
400
300
200
100
0
-0.02
-0.01
0
0.01
0.02

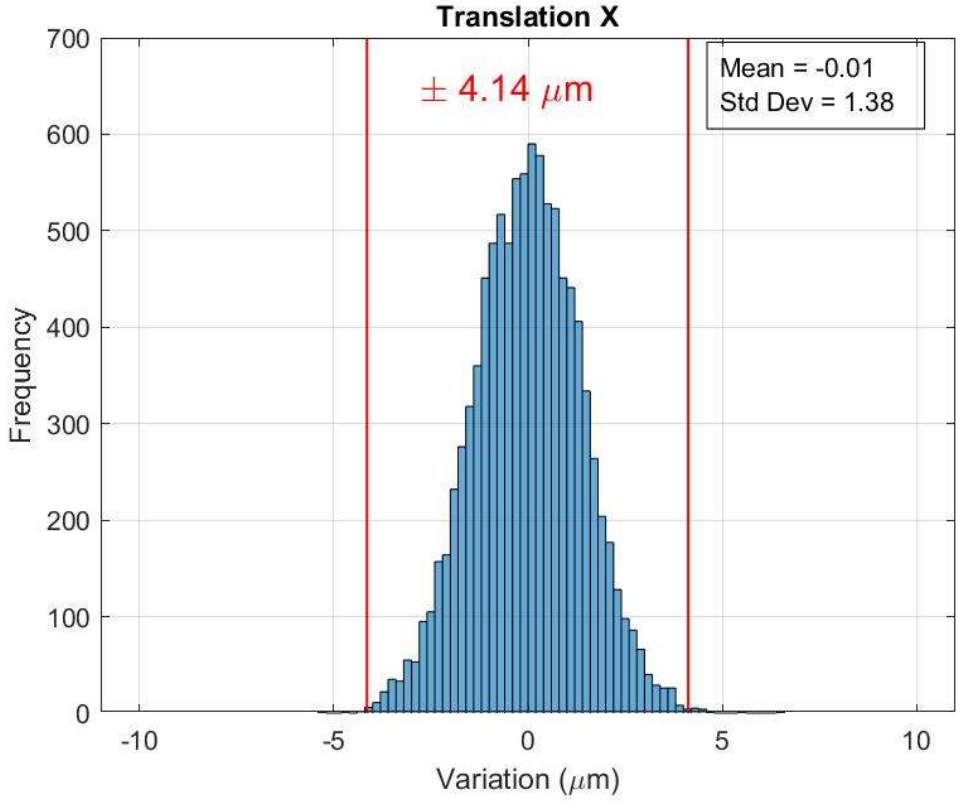
Translation X
± 4.14 μm
Mean = -0.01
Std Dev = 1.38
Frequency
Variation (μm)
700
600
500
400
300
200
100
0
-10
-5
0
5
10

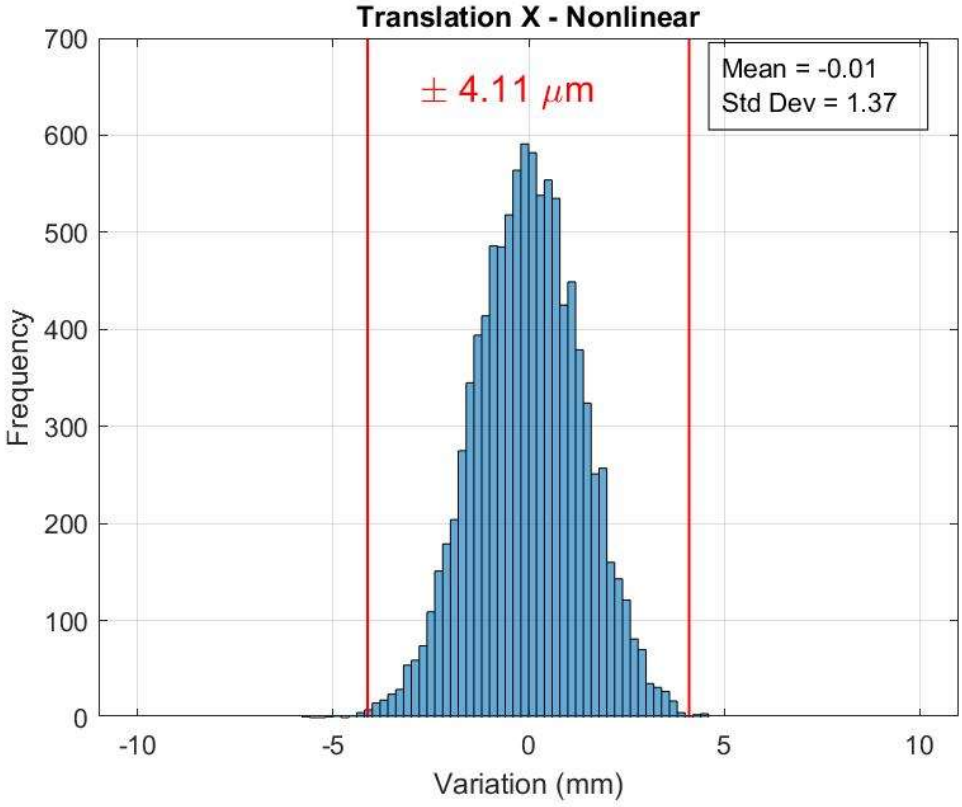
Translation X - Nonlinear
± 4.11 μm
Mean = -0.01
Std Dev = 1.37
Frequency
Variation (mm)
700
600
500
400
300
200
100
0
-10
-5
0
5
10

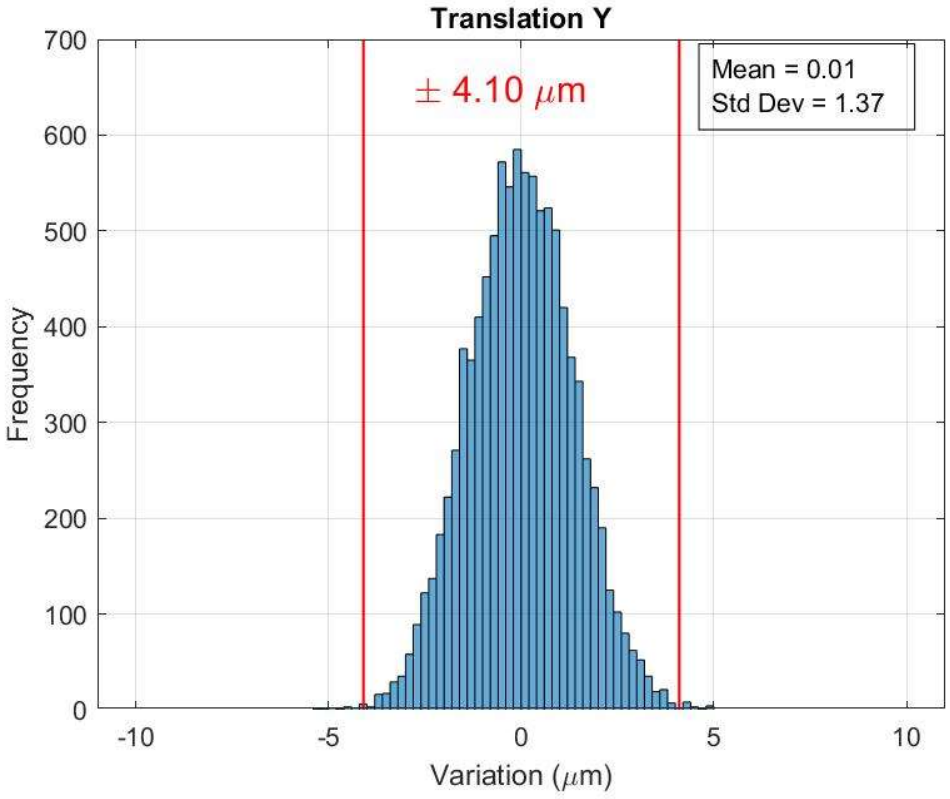
Translation Y
± 4.10 μm
Mean = 0.01
Std Dev = 1.37
Frequency
Variation (μm)
700
600
500
400
300
200
100
0
-10
-5
0
5
10

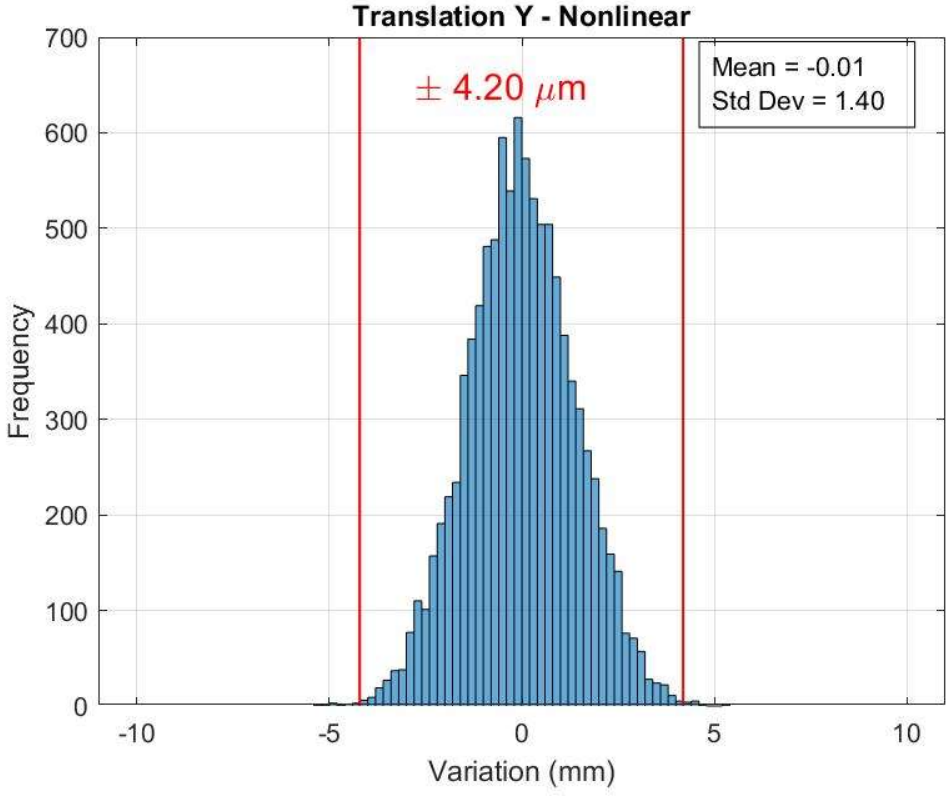
Translation Y - Nonlinear
± 4.20 μm
Mean = -0.01
Std Dev = 1.40
Frequency
Variation (mm)
700
600
500
400
300
200
100
0
-10
-5
0
5
10

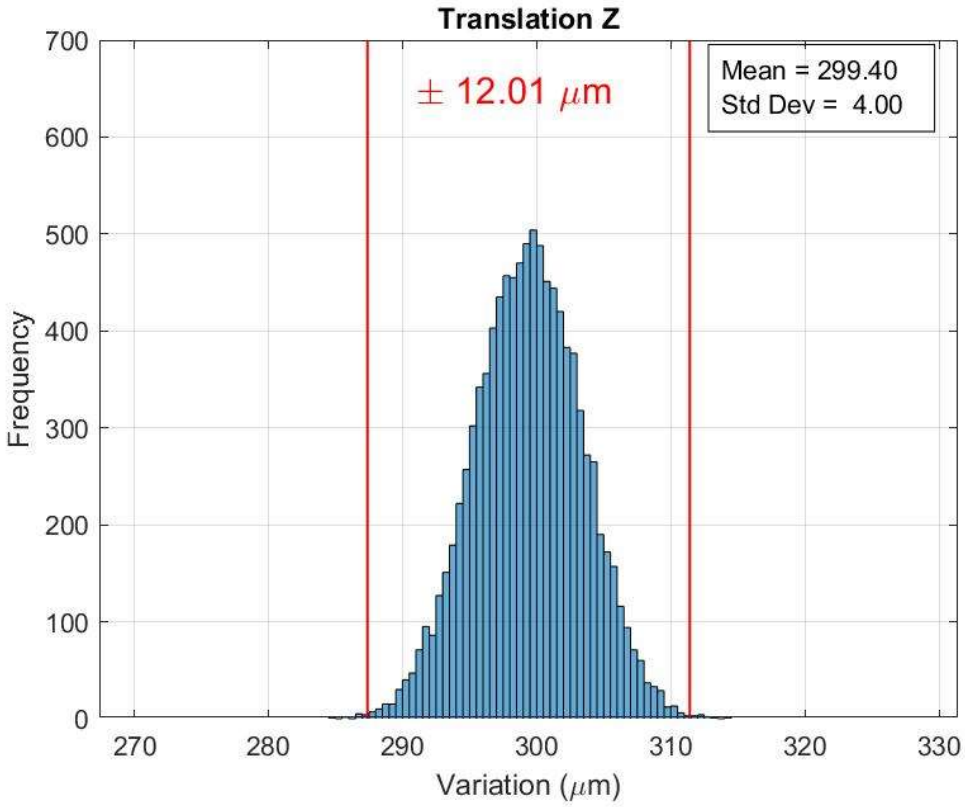
Translation Z
± 12.01 μm
Mean = 299.40
Std Dev = 4.00
Frequency
Variation (μm)
0
100
200
300
400
500
600
700
270
280
290
300
310
320
330

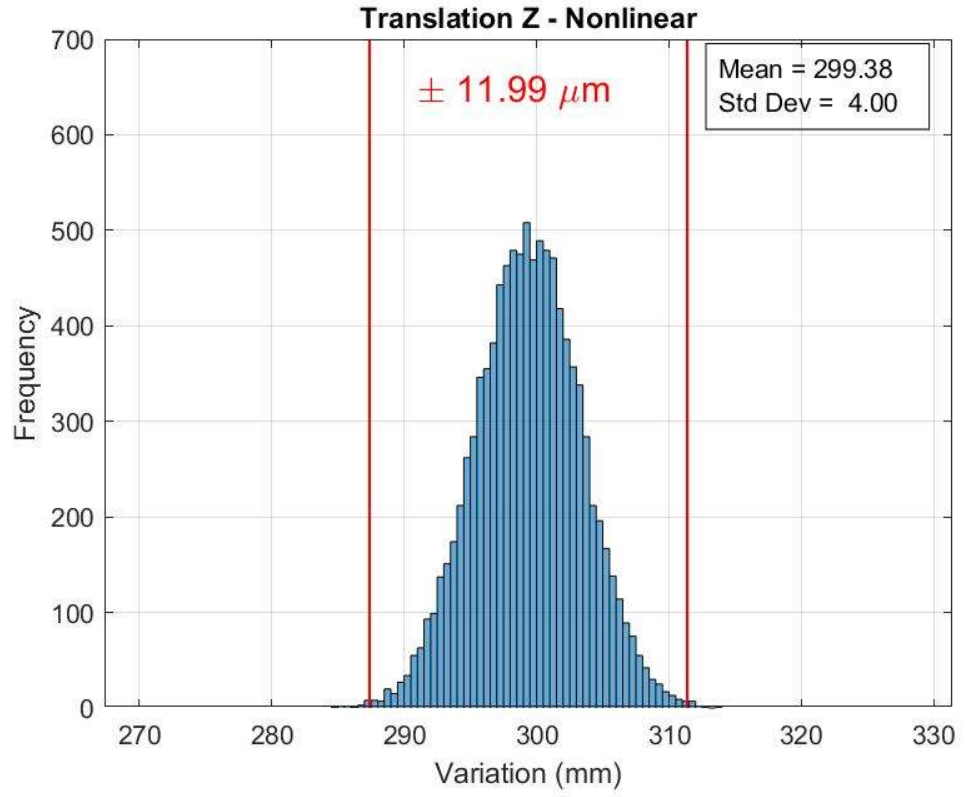
Translation Z - Nonlinear
± 11.99 μm
Mean = 299.38
Std Dev = 4.00
Frequency
Variation (mm)
0
100
200
300
400
500
600
700
270
280
290
300
310
320
330

APPENDIX B: PERCENT CONTRIBUTION CHARTS

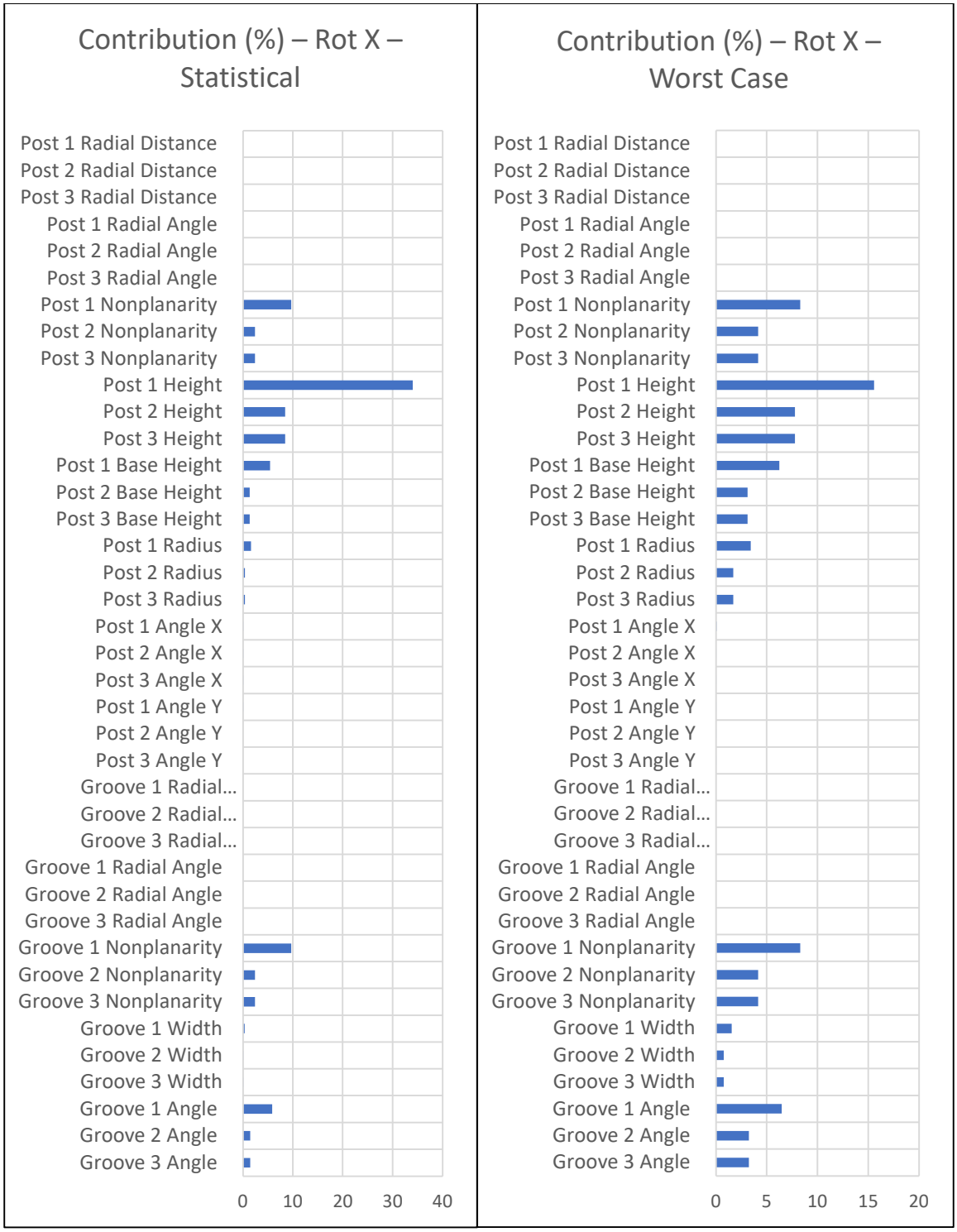

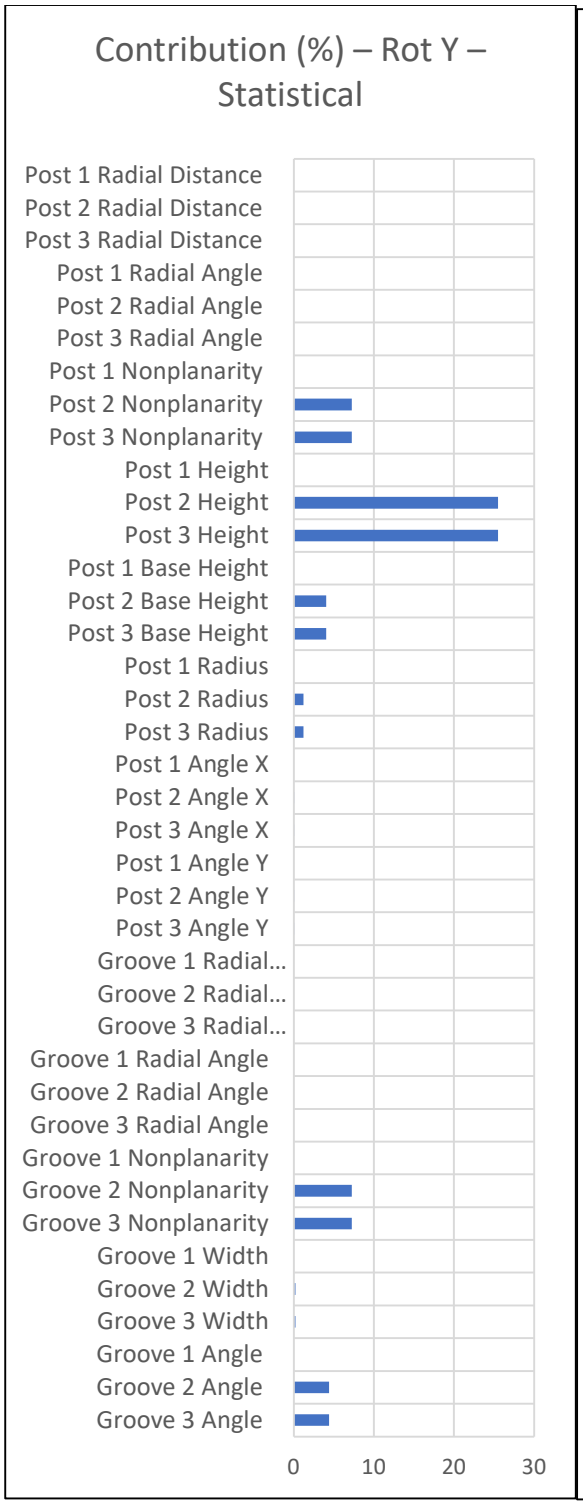
Contribution (%) – Rot Y – Statistical
Post 1 Radial Distance
Post 2 Radial Distance
Post 3 Radial Distance
Post 1 Radial Angle
Post 2 Radial Angle
Post 3 Radial Angle
Post 1 Nonplanarity
Post 2 Nonplanarity
Post 3 Nonplanarity
Post 1 Height
Post 2 Height
Post 3 Height
Post 1 Base Height
Post 2 Base Height
Post 3 Base Height
Post 1 Radius
Post 2 Radius
Post 3 Radius
Post 1 Angle X
Post 2 Angle X
Post 3 Angle X
Post 1 Angle Y
Post 2 Angle Y
Post 3 Angle Y
Groove 1 Radial...
Groove 2 Radial...
Groove 3 Radial...
Groove 1 Radial Angle
Groove 2 Radial Angle
Groove 3 Radial Angle
Groove 1 Nonplanarity
Groove 2 Nonplanarity
Groove 3 Nonplanarity
Groove 1 Width
Groove 2 Width
Groove 3 Width
Groove 1 Angle
Groove 2 Angle
Groove 3 Angle
0
10
20
30

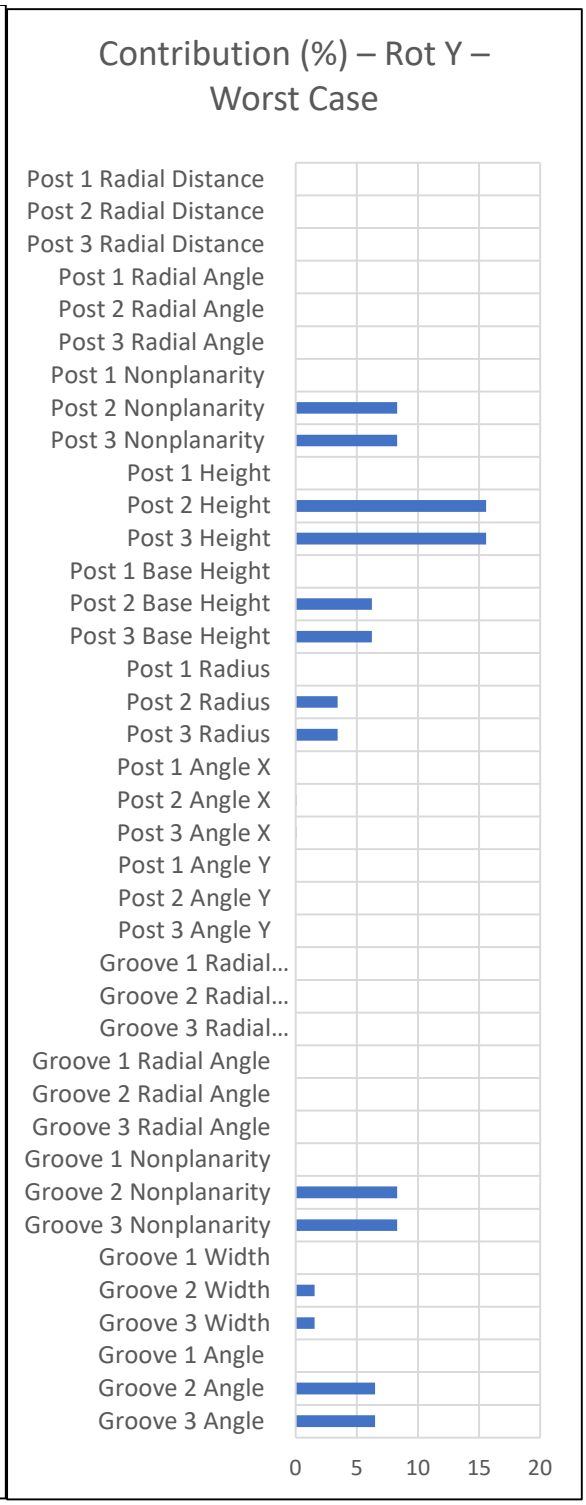
Contribution (%) – Rot Y – Worst Case
Post 1 Radial Distance
Post 2 Radial Distance
Post 3 Radial Distance
Post 1 Radial Angle
Post 2 Radial Angle
Post 3 Radial Angle
Post 1 Nonplanarity
Post 2 Nonplanarity
Post 3 Nonplanarity
Post 1 Height
Post 2 Height
Post 3 Height
Post 1 Base Height
Post 2 Base Height
Post 3 Base Height
Post 1 Radius
Post 2 Radius
Post 3 Radius
Post 1 Angle X
Post 2 Angle X
Post 3 Angle X
Post 1 Angle Y
Post 2 Angle Y
Post 3 Angle Y
Groove 1 Radial...
Groove 2 Radial...
Groove 3 Radial...
Groove 1 Radial Angle
Groove 2 Radial Angle
Groove 3 Radial Angle
Groove 1 Nonplanarity
Groove 2 Nonplanarity
Groove 3 Nonplanarity
Groove 1 Width
Groove 2 Width
Groove 3 Width
Groove 1 Angle
Groove 2 Angle
Groove 3 Angle
0
5
10
15
20


Contribution (%) – Rot Z – Statistical
Post 1 Radial Distance
Post 2 Radial Distance
Post 3 Radial Distance
Post 1 Radial Angle
Post 2 Radial Angle
Post 3 Radial Angle
Post 1 Nonplanarity
Post 2 Nonplanarity
Post 3 Nonplanarity
Post 1 Height
Post 2 Height
Post 3 Height
Post 1 Base Height
Post 2 Base Height
Post 3 Base Height
Post 1 Radius
Post 2 Radius
Post 3 Radius
Post 1 Angle X
Post 2 Angle X
Post 3 Angle X
Post 1 Angle Y
Post 2 Angle Y
Post 3 Angle Y
Groove 1 Radial...
Groove 2 Radial...
Groove 3 Radial...
Groove 1 Radial Angle
Groove 2 Radial Angle
Groove 3 Radial Angle
Groove 1...
Groove 2...
Groove 3...
Groove 1 Width
Groove 2 Width
Groove 3 Width
Groove 1 Angle
Groove 2 Angle
Groove 3 Angle
0
5
10
15
Contribution (%) – Rot Z – Worst Case
Post 1 Radial Distance
Post 2 Radial Distance
Post 3 Radial Distance
Post 1 Radial Angle
Post 2 Radial Angle
Post 3 Radial Angle
Post 1 Nonplanarity
Post 2 Nonplanarity
Post 3 Nonplanarity
Post 1 Height
Post 2 Height
Post 3 Height
Post 1 Base Height
Post 2 Base Height
Post 3 Base Height
Post 1 Radius
Post 2 Radius
Post 3 Radius
Post 1 Angle X
Post 2 Angle X
Post 3 Angle X
Post 1 Angle Y
Post 2 Angle Y
Post 3 Angle Y
Groove 1 Radial...
Groove 2 Radial...
Groove 3 Radial...
Groove 1 Radial Angle
Groove 2 Radial Angle
Groove 3 Radial Angle
Groove 1 Nonplanarity
Groove 2 Nonplanarity
Groove 3 Nonplanarity
Groove 1 Width
Groove 2 Width
Groove 3 Width
Groove 1 Angle
Groove 2 Angle
Groove 3 Angle
0
5
10
15

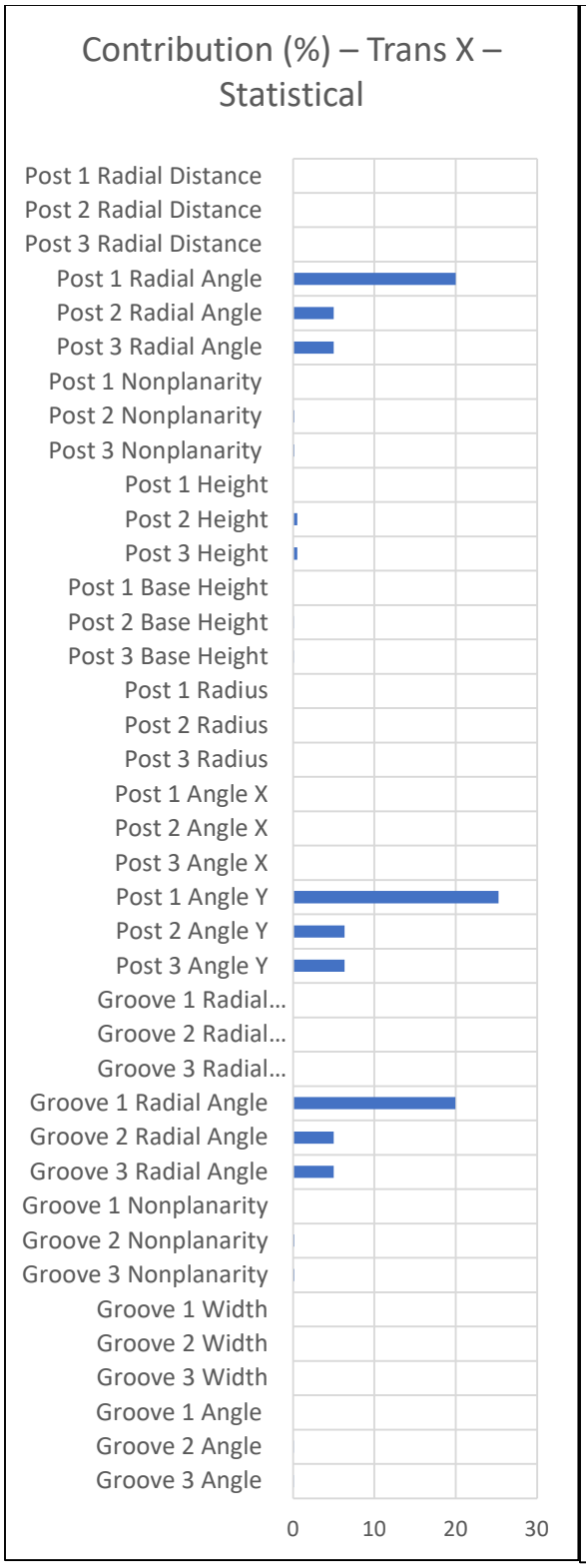
Contribution (%) – Trans X – Statistical
Post 1 Radial Distance
Post 2 Radial Distance
Post 3 Radial Distance
Post 1 Radial Angle
Post 2 Radial Angle
Post 3 Radial Angle
Post 1 Nonplanarity
Post 2 Nonplanarity
Post 3 Nonplanarity
Post 1 Height
Post 2 Height
Post 3 Height
Post 1 Base Height
Post 2 Base Height
Post 3 Base Height
Post 1 Radius
Post 2 Radius
Post 3 Radius
Post 1 Angle X
Post 2 Angle X
Post 3 Angle X
Post 1 Angle Y
Post 2 Angle Y
Post 3 Angle Y
Groove 1 Radial...
Groove 2 Radial...
Groove 3 Radial...
Groove 1 Radial Angle
Groove 2 Radial Angle
Groove 3 Radial Angle
Groove 1 Nonplanarity
Groove 2 Nonplanarity
Groove 3 Nonplanarity
Groove 1 Width
Groove 2 Width
Groove 3 Width
Groove 1 Angle
Groove 2 Angle
Groove 3 Angle
0
10
20
30

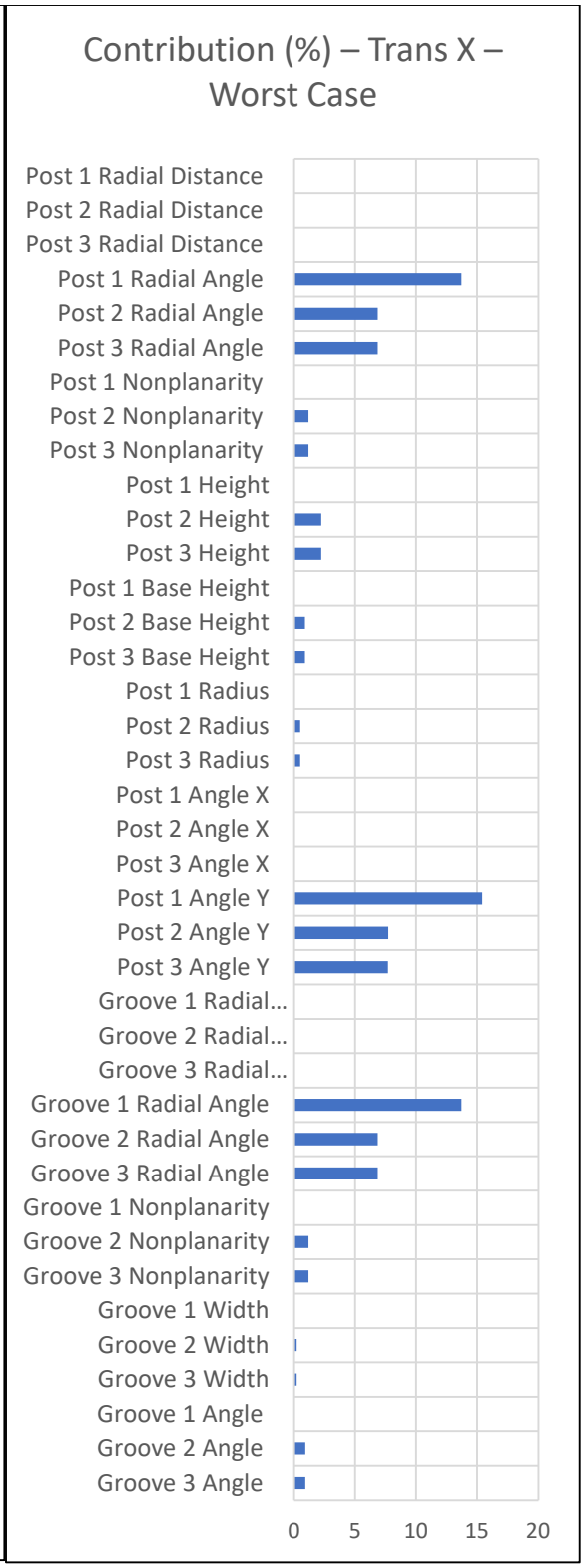
Contribution (%) – Trans X – Worst Case
Post 1 Radial Distance
Post 2 Radial Distance
Post 3 Radial Distance
Post 1 Radial Angle
Post 2 Radial Angle
Post 3 Radial Angle
Post 1 Nonplanarity
Post 2 Nonplanarity
Post 3 Nonplanarity
Post 1 Height
Post 2 Height
Post 3 Height
Post 1 Base Height
Post 2 Base Height
Post 3 Base Height
Post 1 Radius
Post 2 Radius
Post 3 Radius
Post 1 Angle X
Post 2 Angle X
Post 3 Angle X
Post 1 Angle Y
Post 2 Angle Y
Post 3 Angle Y
Groove 1 Radial...
Groove 2 Radial...
Groove 3 Radial...
Groove 1 Radial Angle
Groove 2 Radial Angle
Groove 3 Radial Angle
Groove 1 Nonplanarity
Groove 2 Nonplanarity
Groove 3 Nonplanarity
Groove 1 Width
Groove 2 Width
Groove 3 Width
Groove 1 Angle
Groove 2 Angle
Groove 3 Angle
0
5
10
15
20

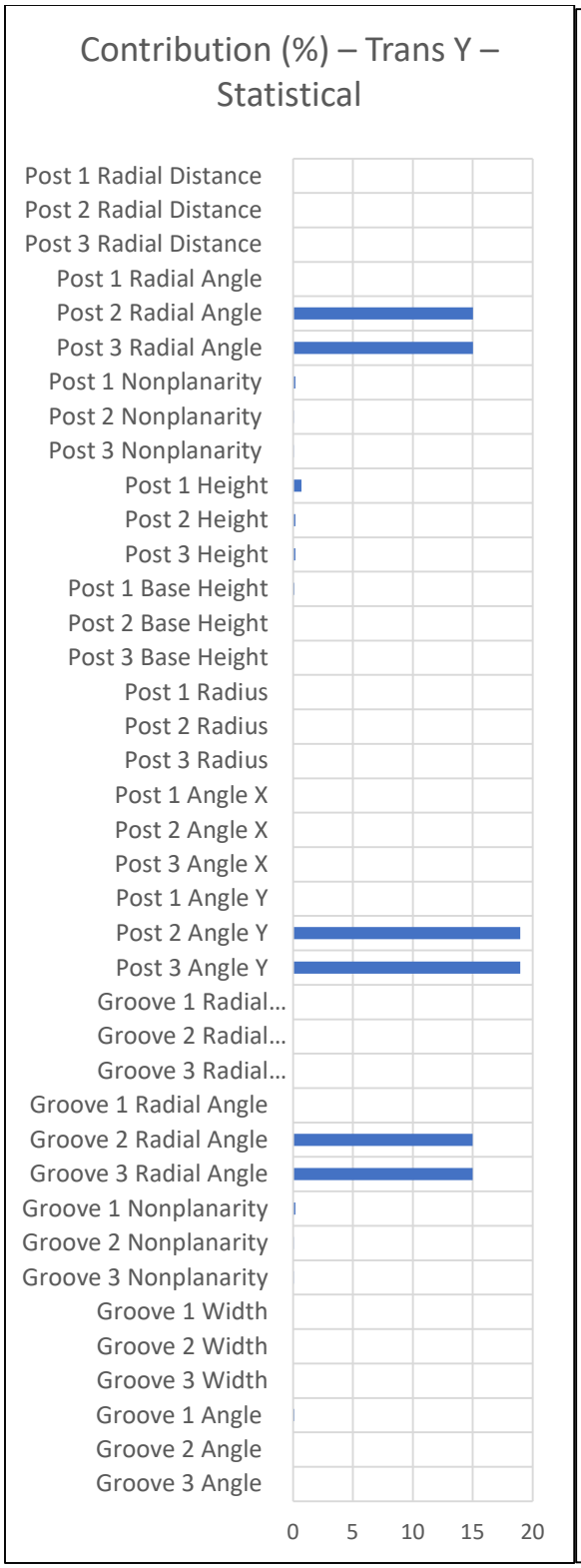
Contribution (%) – Trans Y – Statistical
Post 1 Radial Distance
Post 2 Radial Distance
Post 3 Radial Distance
Post 1 Radial Angle
Post 2 Radial Angle
Post 3 Radial Angle
Post 1 Nonplanarity
Post 2 Nonplanarity
Post 3 Nonplanarity
Post 1 Height
Post 2 Height
Post 3 Height
Post 1 Base Height
Post 2 Base Height
Post 3 Base Height
Post 1 Radius
Post 2 Radius
Post 3 Radius
Post 1 Angle X
Post 2 Angle X
Post 3 Angle X
Post 1 Angle Y
Post 2 Angle Y
Post 3 Angle Y
Groove 1 Radial...
Groove 2 Radial...
Groove 3 Radial...
Groove 1 Radial Angle
Groove 2 Radial Angle
Groove 3 Radial Angle
Groove 1 Nonplanarity
Groove 2 Nonplanarity
Groove 3 Nonplanarity
Groove 1 Width
Groove 2 Width
Groove 3 Width
Groove 1 Angle
Groove 2 Angle
Groove 3 Angle
0
5
10
15
20

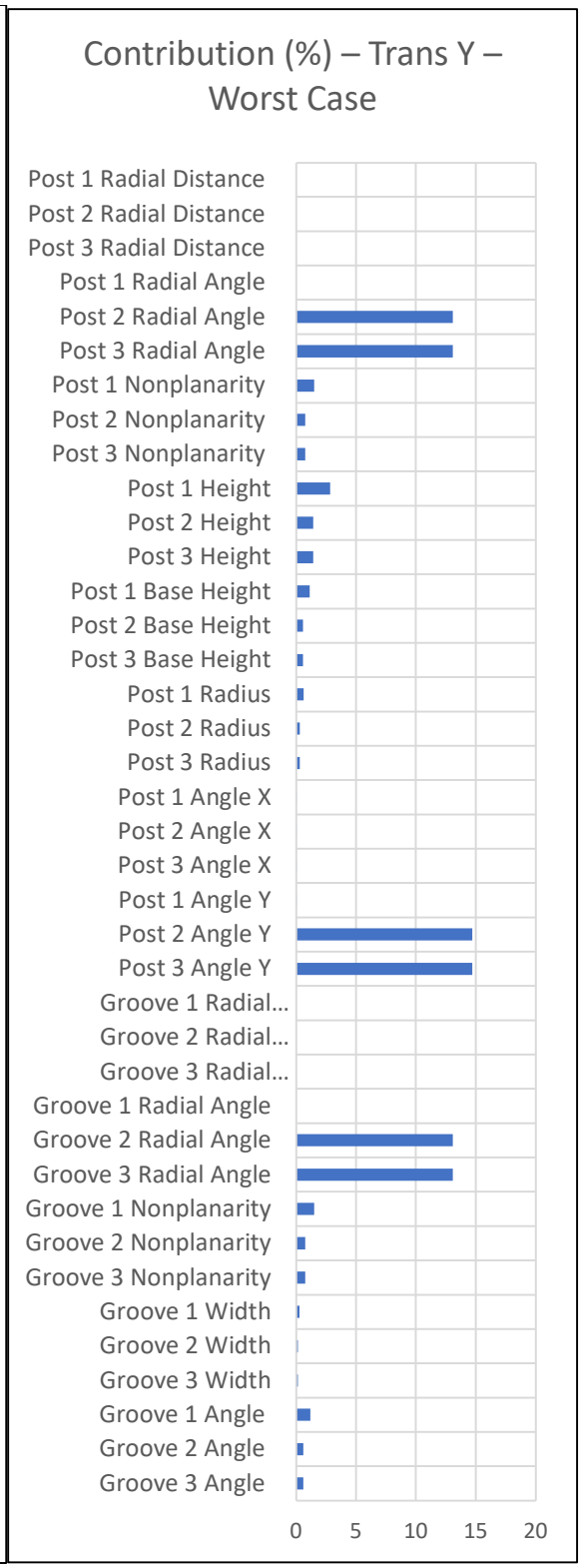
Contribution (%) – Trans Y – Worst Case
Post 1 Radial Distance
Post 2 Radial Distance
Post 3 Radial Distance
Post 1 Radial Angle
Post 2 Radial Angle
Post 3 Radial Angle
Post 1 Nonplanarity
Post 2 Nonplanarity
Post 3 Nonplanarity
Post 1 Height
Post 2 Height
Post 3 Height
Post 1 Base Height
Post 2 Base Height
Post 3 Base Height
Post 1 Radius
Post 2 Radius
Post 3 Radius
Post 1 Angle X
Post 2 Angle X
Post 3 Angle X
Post 1 Angle Y
Post 2 Angle Y
Post 3 Angle Y
Groove 1 Radial...
Groove 2 Radial...
Groove 3 Radial...
Groove 1 Radial Angle
Groove 2 Radial Angle
Groove 3 Radial Angle
Groove 1 Nonplanarity
Groove 2 Nonplanarity
Groove 3 Nonplanarity
Groove 1 Width
Groove 2 Width
Groove 3 Width
Groove 1 Angle
Groove 2 Angle
Groove 3 Angle
0
5
10
15
20


Contribution (%) – Trans Z – Statistical
Post 1 Radial Distance
Post 2 Radial Distance
Post 3 Radial Distance
Post 1 Radial Angle
Post 2 Radial Angle
Post 3 Radial Angle
Post 1 Nonplanarity
Post 2 Nonplanarity
Post 3 Nonplanarity
Post 1 Height
Post 2 Height
Post 3 Height
Post 1 Base Height
Post 2 Base Height
Post 3 Base Height
Post 1 Radius
Post 2 Radius
Post 3 Radius
Post 1 Angle X
Post 2 Angle X
Post 3 Angle X
Post 1 Angle Y
Post 2 Angle Y
Post 3 Angle Y
Groove 1 Radial...
Groove 2 Radial...
Groove 3 Radial...
Groove 1 Radial Angle
Groove 2 Radial Angle
Groove 3 Radial Angle
Groove 1 Nonplanarity
Groove 2 Nonplanarity
Groove 3 Nonplanarity
Groove 1 Width
Groove 2 Width
Groove 3 Width
Groove 1 Angle
Groove 2 Angle
Groove 3 Angle
0
5
10
15
20
Contribution (%) – Trans Z – Worst Case
Post 1 Radial Distance
Post 2 Radial Distance
Post 3 Radial Distance
Post 1 Radial Angle
Post 2 Radial Angle
Post 3 Radial Angle
Post 1 Nonplanarity
Post 2 Nonplanarity
Post 3 Nonplanarity
Post 1 Height
Post 2 Height
Post 3 Height
Post 1 Base Height
Post 2 Base Height
Post 3 Base Height
Post 1 Radius
Post 2 Radius
Post 3 Radius
Post 1 Angle X
Post 2 Angle X
Post 3 Angle X
Post 1 Angle Y
Post 2 Angle Y
Post 3 Angle Y
Groove 1 Radial...
Groove 2 Radial...
Groove 3 Radial...
Groove 1 Radial Angle
Groove 2 Radial Angle
Groove 3 Radial Angle
Groove 1 Nonplanarity
Groove 2 Nonplanarity
Groove 3 Nonplanarity
Groove 1 Width
Groove 2 Width
Groove 3 Width
Groove 1 Angle
Groove 2 Angle
Groove 3 Angle
0
5
10
15

APPENDIX C: GRAPHS SHOWING EFFECT OF DECREASING POST TOLERANCES

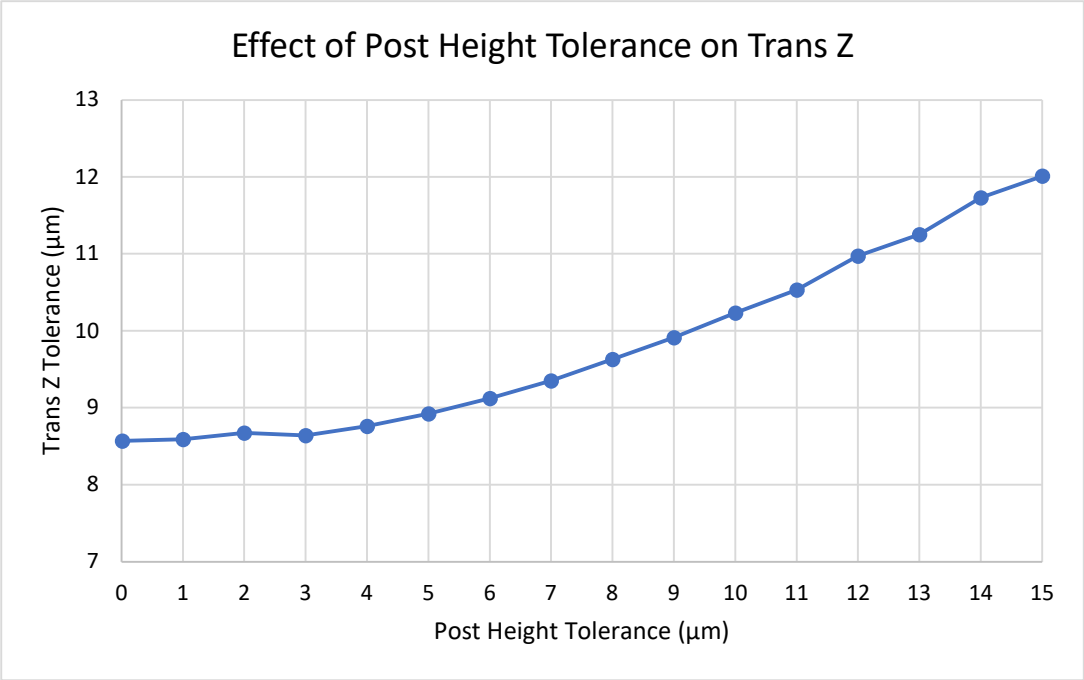

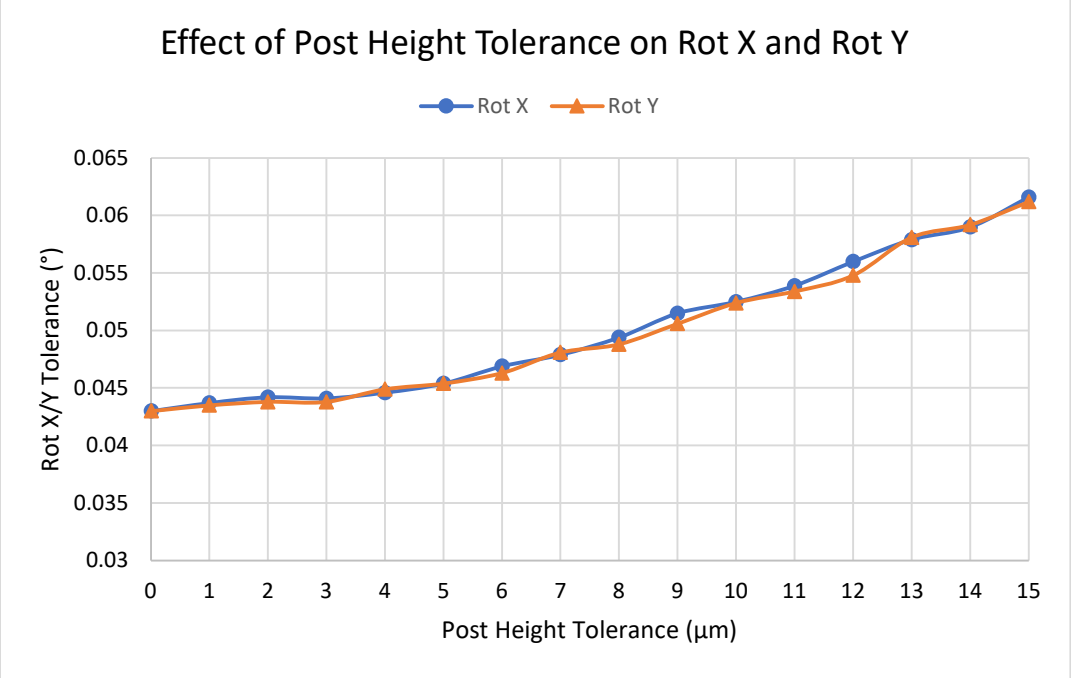

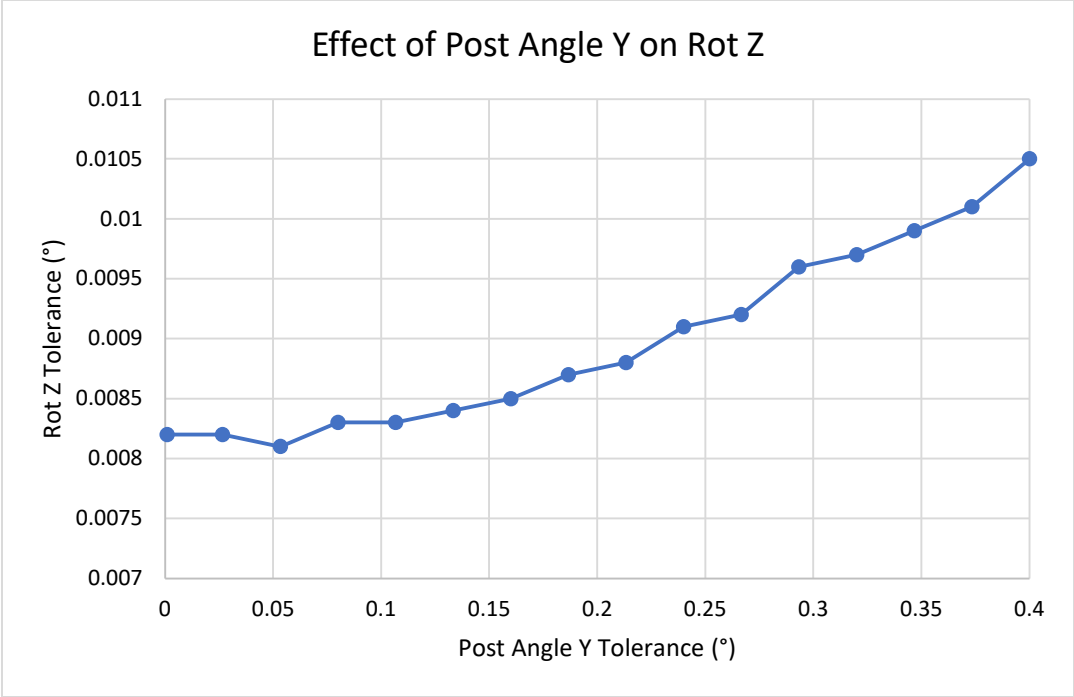
Effect of Post Angle Y on Rot Z
Rot Z Tolerance (°)
0.011
0.0105
0.01
0.0095
0.009
0.0085
0.008
0.0075
0.007
0
0.05
0.1
0.15
0.2
0.25
0.3
0.35
0.4
Post Angle Y Tolerance (°)

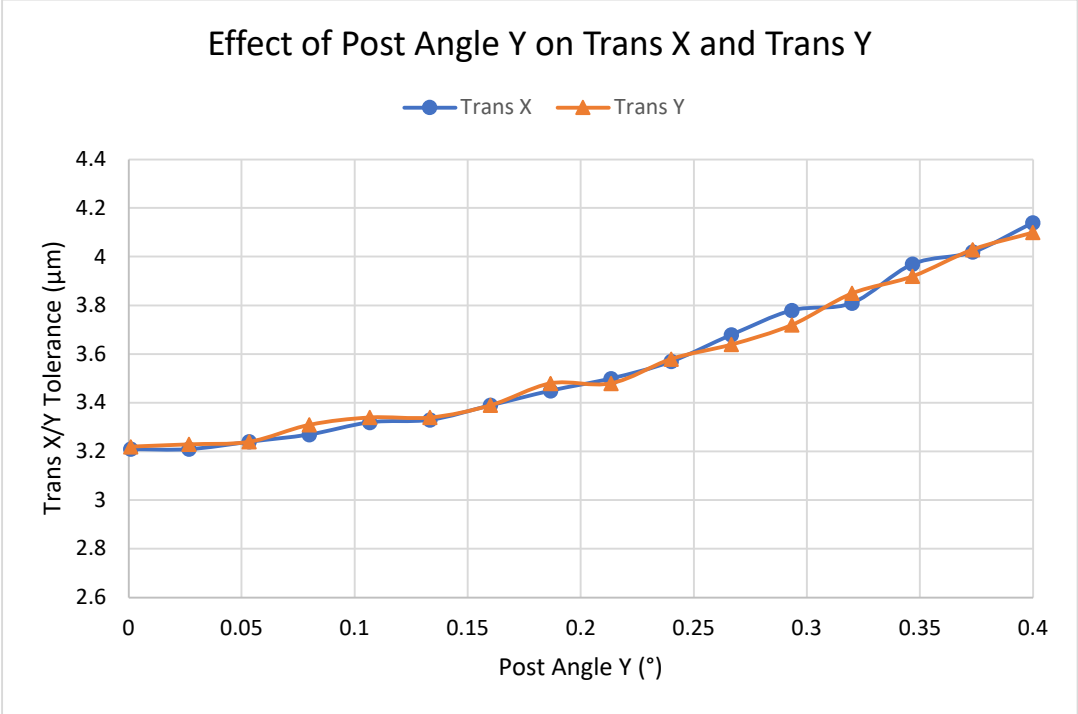
Effect of Post Angle Y on Trans X and Trans Y
Trans X
Trans Y
Trans X/Y Tolerance (µm)
4.4
4.2
4
3.8
3.6
3.4
3.2
3
2.8
2.6
0
0.05
0.1
0.15
0.2
0.25
0.3
0.35
0.4
Post Angle Y (°)

APPENDIX D: LINEAR MONTE CARLO SIMULATION MATLAB CODE

```
% Tolerance Analysis - Linear Monte Carlo Simulation
% Linear calculation of assembly variables from random
values of component dimensions
% Component dimension values normally distributed with
tolerance equal to 3 sigma range
% Can be modified to perform sensitivity analysis by
setting all dimension values equal to their mean, and
then manually adjusting one at a time and recording
effect on assembly variables

% All units in mm unless specified otherwise

for i = 1:10000

% Random dimension values following normal dist with
tolerance equal to 3 sigma range
% Given by normrnd(mean, sigma, size)
% Example: 3*sigma = 0.003  =>  sigma = 0.003/3
PostRadDist = normrnd(15.908, (.003/3), [3,1]);
% 15.908 +- 0.003
PostRadAngle = normrnd(0, (.01/3), [3,1]);
%  0.0 +- 0.01 deg
PostNonplan = normrnd(-.003, (.008/3), [3,1]);
% -0.003 +- 0.008
PostHeight = normrnd(.932, (.015/3), [3,1]);
%  0.932 +- 0.015
PostBaseHeight = normrnd(.103, (.006/3), [3,1]);
%  0.103 +- 0.006
PostRadius = normrnd(.485, (.008/3), [3,1]);
%  0.485 +- 0.008
PostAngleX = normrnd(-1.4, (.4/3), [3,1]);
% -1.4 +- 0.4 deg
PostAngleY = normrnd(0, (0.4/3), [3,1]);
%  0.0 +- 0.4 deg

GrooveRadDist = normrnd(15.908, (.003/3), [3,1]);
% 15.908 +- 0.003
GrooveRadAngle = normrnd(0, (.01/3), [3,1]);
%  0.0 +- 0.01 deg
GrooveNonplan = normrnd(-.003, (.008/3), [3,1]);
% -0.003 +- 0.008
```

```
GrooveWidth = normrnd(1.877, (.003/3), [3,1]);
%  1.877 +- 0.003
GrooveAngle = normrnd(44.9, (.3/3), [3,1]);
% 44.9 +- 0.3 deg

% Elements of vector from Upper Module to center of
Post 1
PostCen1X = (-sqrt(PostRadDist(1)^2-
PostNonplan(1)^2)*sind(PostRadAngle(1))) -
((PostHeight(1)-PostRadius(1))*sind(PostAngleY(1)));
PostCen1Y = (sqrt(PostRadDist(1)^2-
PostNonplan(1)^2)*cosd(PostRadAngle(1))) +
((PostHeight(1)-PostRadius(1))*sind(PostAngleX(1)));
PostCen1Z = PostNonplan(1)-PostBaseHeight(1)-
(((PostHeight(1)-
PostRadius(1))*cosd(PostAngleX(1)))*cosd(PostAngleY(1))
);

PostCen2X = PostCen1X;
PostCen2Y = PostCen1Y;
PostCen2Z = PostCen1Z;

% Elements of vector from Upper Module to center of
Post 2
PostCen3_X = (-sqrt(PostRadDist(2)^2-
PostNonplan(2)^2)*sind(PostRadAngle(2))) -
((PostHeight(2)-PostRadius(2))*sind(PostAngleY(2)));
PostCen3_Y = (sqrt(PostRadDist(2)^2-
PostNonplan(2)^2)*cosd(PostRadAngle(2))) +
((PostHeight(2)-PostRadius(2))*sind(PostAngleX(2)));
PostCen3_Z = PostNonplan(2)-PostBaseHeight(2)-
(((PostHeight(2)-
PostRadius(2))*cosd(PostAngleX(2)))*cosd(PostAngleY(2))
);
CenterPost2 = [cosd(120) -sind(120) 0 0;sind(120)
cosd(120) 0 0;0 0 1 0; 0 0 0
1]*[PostCen3_X;PostCen3_Y;PostCen3_Z;1];

PostCen3X = CenterPost2(1);
PostCen3Y = CenterPost2(2);
PostCen3Z = CenterPost2(3);

PostCen4X = PostCen3X;
PostCen4Y = PostCen3Y;
```

```
PostCen4Z = PostCen3Z;

% Elements of vector from Upped Module to center of
Post 3
PostCen5_X = (-sqrt(PostRadDist(3)^2-
PostNonplan(3)^2)*sind(PostRadAngle(3))) -
((PostHeight(3)-PostRadius(3))*sind(PostAngleY(3)));
PostCen5_Y = (sqrt(PostRadDist(3)^2-
PostNonplan(3)^2)*cosd(PostRadAngle(3))) +
((PostHeight(3)-PostRadius(3))*sind(PostAngleX(3)));
PostCen5_Z = PostNonplan(3)-PostBaseHeight(3)-
(((PostHeight(3)-
PostRadius(3))*cosd(PostAngleX(3)))*cosd(PostAngleY(3))
);
CenterPost3 = [cosd(240) -sind(240) 0 0;sind(240)
cosd(240) 0 0;0 0 1 0; 0 0 0
1]*[PostCen5_X;PostCen5_Y;PostCen5_Z;1];

PostCen5X = CenterPost3(1);
PostCen5Y = CenterPost3(2);
PostCen5Z = CenterPost3(3);

PostCen6X = PostCen5X;
PostCen6Y = PostCen5Y;
PostCen6Z = PostCen5Z;

% Elements of vector normal to Groove Surface 1
Norm1X = -
((PostRadius(1)*sind(GrooveAngle(1)))*cosd(GrooveRadAng
le(1)))/PostRadius(1);
Norm1Y = -
((PostRadius(1)*sind(GrooveAngle(1)))*sind(GrooveRadAng
le(1)))/PostRadius(1);
Norm1Z = cosd(GrooveAngle(1));

% Elements of vector normal to Groove Surface 2
Norm2X =
((PostRadius(1)*sind(GrooveAngle(1)))*cosd(GrooveRadAng
le(1)))/PostRadius(1);
Norm2Y =
((PostRadius(1)*sind(GrooveAngle(1)))*sind(GrooveRadAng
le(1)))/PostRadius(1);
Norm2Z = cosd(GrooveAngle(1));
```

```
% Elements of vector normal to Groove Surface 3
Norm3X =
((PostRadius(2)*sind(GrooveAngle(2)))*sind(GrooveRadAng
le(2)+30))/PostRadius(2);
Norm3Y = -
((PostRadius(2)*sind(GrooveAngle(2)))*cosd(GrooveRadAng
le(2)+30))/PostRadius(2);
Norm3Z = cosd(GrooveAngle(2));

% Elements of vector normal to Groove Surface 4
Norm4X = -
((PostRadius(2)*sind(GrooveAngle(2)))*sind(GrooveRadAng
le(2)+30))/PostRadius(2);
Norm4Y =
((PostRadius(2)*sind(GrooveAngle(2)))*cosd(GrooveRadAng
le(2)+30))/PostRadius(2);
Norm4Z = cosd(GrooveAngle(2));

% Elements of vector normal to Groove Surface 5
Norm5X = ((PostRadius(3)*sind(GrooveAngle(3)))*sind(-
GrooveRadAngle(3)+30))/PostRadius(3);
Norm5Y = ((PostRadius(3)*sind(GrooveAngle(3)))*cosd(-
GrooveRadAngle(3)+30))/PostRadius(3);
Norm5Z = cosd(GrooveAngle(3));

% Elements of vector normal to Groove Surface 6
Norm6X = -((PostRadius(3)*sind(GrooveAngle(3)))*sind(-
GrooveRadAngle(3)+30))/PostRadius(3);
Norm6Y = -((PostRadius(3)*sind(GrooveAngle(3)))*cosd(-
GrooveRadAngle(3)+30))/PostRadius(3);
Norm6Z = cosd(GrooveAngle(3));

% Elements of vector from Lower Module to point on
Grove Surface 1
Pg1X = (-sqrt(GrooveRadDist(1)^2-
GrooveNonplan(1)^2)*sind(GrooveRadAngle(1))) +
((GrooveWidth(1)/2)*cosd(GrooveRadAngle(1)));
Pg1Y = (sqrt(GrooveRadDist(1)^2-
GrooveNonplan(1)^2)*cosd(GrooveRadAngle(1))) +
((GrooveWidth(1)/2)*sind(GrooveRadAngle(1)));
Pg1Z = GrooveNonplan(1);
```

```
% Elements of vector from Lower Module to point on
Grove Surface 2
Pg2X = (-sqrt(GrooveRadDist(1)^2-
GrooveNonplan(1)^2)*sind(GrooveRadAngle(1))) + ((-
GrooveWidth(1)/2)*cosd(GrooveRadAngle(1)));
Pg2Y = (sqrt(GrooveRadDist(1)^2-
GrooveNonplan(1)^2)*cosd(GrooveRadAngle(1))) + ((-
GrooveWidth(1)/2)*sind(GrooveRadAngle(1)));
Pg2Z = GrooveNonplan(1);

% Elements of vector from Lower Module to point on
Grove Surface 3
Pg3X = (-sqrt(GrooveRadDist(2)^2-
GrooveNonplan(2)^2)*cosd(GrooveRadAngle(2)+30)) + ((-
GrooveWidth(2)/2)*sind(GrooveRadAngle(2)+30));
Pg3Y = (-sqrt(GrooveRadDist(2)^2-
GrooveNonplan(2)^2)*sind(GrooveRadAngle(2)+30)) +
((GrooveWidth(2)/2)*cosd(GrooveRadAngle(2)+30));
Pg3Z = GrooveNonplan(2);

% Elements of vector from Lower Module to point on
Grove Surface 4
Pg4X = (-sqrt(GrooveRadDist(2)^2-
GrooveNonplan(2)^2)*cosd(GrooveRadAngle(2)+30)) +
((GrooveWidth(2)/2)*sind(GrooveRadAngle(2)+30));
Pg4Y = (-sqrt(GrooveRadDist(2)^2-
GrooveNonplan(2)^2)*sind(GrooveRadAngle(2)+30)) + ((-
GrooveWidth(2)/2)*cosd(GrooveRadAngle(2)+30));
Pg4Z = GrooveNonplan(2);

% Elements of vector from Lower Module to point on
Grove Surface 5
Pg5X = (sqrt(GrooveRadDist(3)^2-
GrooveNonplan(3)^2)*cosd(-GrooveRadAngle(3)+30)) + ((-
GrooveWidth(3)/2)*sind(-GrooveRadAngle(3)+30));
Pg5Y = (-sqrt(GrooveRadDist(3)^2-
GrooveNonplan(3)^2)*sind(-GrooveRadAngle(3)+30)) + ((-
GrooveWidth(3)/2)*cosd(-GrooveRadAngle(3)+30));
Pg5Z = GrooveNonplan(3);

% Elements of vector from Lower Module to point on
Grove Surface 6
```

```
Pg6X = (sqrt(GrooveRadDist(3)^2-
GrooveNonplan(3)^2)*cosd(-GrooveRadAngle(3)+30)) +
((GrooveWidth(3)/2)*sind(-GrooveRadAngle(3)+30));
Pg6Y = (-sqrt(GrooveRadDist(3)^2-
GrooveNonplan(3)^2)*sind(-GrooveRadAngle(3)+30)) +
((GrooveWidth(3)/2)*cosd(-GrooveRadAngle(3)+30));
Pg6Z = GrooveNonplan(3);

% Coefficients for equation or matrix row 1
Ctx1 = (-PostCen1Z*Norm1Y) + (PostCen1Y*Norm1Z);
Cty1 = (PostCen1Z*Norm1X) + (-PostCen1X*Norm1Z);
Ctz1 = (-PostCen1Y*Norm1X) + (PostCen1X*Norm1Y);
Cdx1 = Norm1X;
Cdy1 = Norm1Y;
Cdz1 = Norm1Z;
C1 = (PostCen1X*Norm1X) + ((-
PostRadius(1)*Norm1X)*Norm1X) + (-Pg1X*Norm1X) +
(PostCen1Y*Norm1Y) + ((-PostRadius(1)*Norm1Y)*Norm1Y) +
(-Pg1Y*Norm1Y) + (PostCen1Z*Norm1Z) + ((-
PostRadius(1)*Norm1Z)*Norm1Z) + (-Pg1Z*Norm1Z);

% Coefficients for equation or matrix row 2
Ctx2 = (-PostCen2Z*Norm2Y) + (PostCen2Y*Norm2Z);
Cty2 = (PostCen2Z*Norm2X) + (-PostCen2X*Norm2Z);
Ctz2 = (-PostCen2Y*Norm2X) + (PostCen2X*Norm2Y);
Cdx2 = Norm2X;
Cdy2 = Norm2Y;
Cdz2 = Norm2Z;
C2 = (PostCen2X*Norm2X) + ((-
PostRadius(1)*Norm2X)*Norm2X) + (-Pg2X*Norm2X) +
(PostCen2Y*Norm2Y) + ((-PostRadius(1)*Norm2Y)*Norm2Y) +
(-Pg2Y*Norm2Y) + (PostCen2Z*Norm2Z) + ((-
PostRadius(1)*Norm2Z)*Norm2Z) + (-Pg2Z*Norm2Z);

% Coefficients for equation or matrix row 3
Ctx3 = (-PostCen3Z*Norm3Y) + (PostCen3Y*Norm3Z);
Cty3 = (PostCen3Z*Norm3X) + (-PostCen3X*Norm3Z);
Ctz3 = (-PostCen3Y*Norm3X) + (PostCen3X*Norm3Y);
Cdx3 = Norm3X;
Cdy3 = Norm3Y;
Cdz3 = Norm3Z;
C3 = (PostCen3X*Norm3X) + ((-
PostRadius(2)*Norm3X)*Norm3X) + (-Pg3X*Norm3X) +
(PostCen3Y*Norm3Y) + ((-PostRadius(2)*Norm3Y)*Norm3Y) +
```

```
(-Pg3Y*Norm3Y) + (PostCen3Z*Norm3Z) + ((-
PostRadius(2)*Norm3Z)*Norm3Z) + (-Pg3Z*Norm3Z);

% Coefficients for equation or matrix row 4
Ctx4 = (-PostCen4Z*Norm4Y) + (PostCen4Y*Norm4Z);
Cty4 = (PostCen4Z*Norm4X) + (-PostCen4X*Norm4Z);
Ctz4 = (-PostCen4Y*Norm4X) + (PostCen4X*Norm4Y);
Cdx4 = Norm4X;
Cdy4 = Norm4Y;
Cdz4 = Norm4Z;
C4 = (PostCen4X*Norm4X) + ((-
PostRadius(2)*Norm4X)*Norm4X) + (-Pg4X*Norm4X) +
(PostCen4Y*Norm4Y) + ((-PostRadius(2)*Norm4Y)*Norm4Y) +
(-Pg4Y*Norm4Y) + (PostCen4Z*Norm4Z) + ((-
PostRadius(2)*Norm4Z)*Norm4Z) + (-Pg4Z*Norm4Z);

% Coefficients for equation or matrix row 5
Ctx5 = (-PostCen5Z*Norm5Y) + (PostCen5Y*Norm5Z);
Cty5 = (PostCen5Z*Norm5X) + (-PostCen5X*Norm5Z);
Ctz5 = (-PostCen5Y*Norm5X) + (PostCen5X*Norm5Y);
Cdx5 = Norm5X;
Cdy5 = Norm5Y;
Cdz5 = Norm5Z;
C5 = (PostCen5X*Norm5X) + ((-
PostRadius(3)*Norm5X)*Norm5X) + (-Pg5X*Norm5X) +
(PostCen5Y*Norm5Y) + ((-PostRadius(3)*Norm5Y)*Norm5Y) +
(-Pg5Y*Norm5Y) + (PostCen5Z*Norm5Z) + ((-
PostRadius(3)*Norm5Z)*Norm5Z) + (-Pg5Z*Norm5Z);

% Coefficients for equation or matrix row 6
Ctx6 = (-PostCen6Z*Norm6Y) + (PostCen6Y*Norm6Z);
Cty6 = (PostCen6Z*Norm6X) + (-PostCen6X*Norm6Z);
Ctz6 = (-PostCen6Y*Norm6X) + (PostCen6X*Norm6Y);
Cdx6 = Norm6X;
Cdy6 = Norm6Y;
Cdz6 = Norm6Z;
C6 = (PostCen6X*Norm6X) + ((-
PostRadius(3)*Norm6X)*Norm6X) + (-Pg6X*Norm6X) +
(PostCen6Y*Norm6Y) + ((-PostRadius(3)*Norm6Y)*Norm6Y) +
(-Pg6Y*Norm6Y) + (PostCen6Z*Norm6Z) + ((-
PostRadius(3)*Norm6Z)*Norm6Z) + (-Pg6Z*Norm6Z);

% Matrix of variable coefficients
```

```
M = [Ctx1 Cty1 Ctz1 Cdx1 Cdy1 Cdz1;Ctx2 Cty2 Ctz2 Cdx2
Cdy2 Cdz2;Ctx3 Cty3 Ctz3 Cdx3 Cdy3 Cdz3;Ctx4 Cty4 Ctz4
Cdx4 Cdy4 Cdz4;Ctx5 Cty5 Ctz5 Cdx5 Cdy5 Cdz5;Ctx6 Cty6
Ctz6 Cdx6 Cdy6 Cdz6];

% Vector of constants
V = [-C1;-C2;-C3;-C4;-C5;-C6];

% Calculation of assembly variation values
X = linsolve(M,V);

% Conversion of rotational values from radians to
degrees
X(1) = rad2deg(X(1));
X(2) = rad2deg(X(2));
X(3) = rad2deg(X(3));
X(4) = X(4)*1000;
X(5) = X(5)*1000;
X(6) = X(6)*1000;

% Writing each variation value to a separate vector
Rotation_X(i,1)= X(1);
Rotation_Y(i,1)= X(2);
Rotation_Z(i,1)= X(3);
Translation_X(i,1)= X(4);
Translation_Y(i,1)= X(5);
Translation_Z(i,1)= X(6);

Loop_Count=i;

end

% Save each vector of assembly variation values to a
text file
save RotationX.txt Rotation_X -ascii
save RotationY.txt Rotation_Y -ascii
save RotationZ.txt Rotation_Z -ascii
save TranslationX.txt Translation_X -ascii
save TranslationY.txt Translation_Y -ascii
save TranslationZ.txt Translation_Z -ascii

% Calculate standard deviation of each assembly
variable
stdX = std(Rotation_X);
```

```
stdY = std(Rotation_Y);
stdZ = std(Rotation_Z);
stdTX = std(Translation_X);
stdTY = std(Translation_Y);
stdTZ = std(Translation_Z);

% Calculate tolerance of each assembly variable
assuming the same 3 sigma range used for component
dimensions
tolX = 3*stdX
tolY = 3*stdY
tolZ = 3*stdZ
tolTX = 3*stdTX
tolTY = 3*stdTY
tolTZ = 3*stdTZ

% var(Rotation_X)
% var(Rotation_Y)
% var(Rotation_Z)
% var(Translation_X)
% var(Translation_Y)
% var(Translation_Z)

% Graphs showing distribution of assembly variation
values with mean and
%  standard deviation values and tolerances shown by
red lines
meanX = mean(Rotation_X);
hX = histogram(Rotation_X);
grid on
mnXlabel=sprintf('Mean = %5.4f', meanX);
stdXlabel=sprintf('Std Dev = %5.4f', stdX);
h=annotation('textbox',[0.68 0.82 0.1 0.1]);
set(h,'String',{mnXlabel, stdXlabel});
txt = ['\pm ' sprintf('%5.4f', tolX) ' deg'];
text(-.15,650,txt,'FontSize',14,'Color','r')
title('Rotation X');
xlabel('Variation (deg)');
ylabel('Frequency');
xlim([-.18 .18]);
ylim([0 800]);
line([meanX-tolX, meanX-tolX], ylim, 'Color', 'r',
'LineWidth', 1);
```

```
line([meanX+tolX, meanX+tolX], ylim, 'Color', 'r',
'LineWidth', 1);
savename1 = 'histRotX.jpg';
saveas(hX, savename1, 'jpg');

meanY = mean(Rotation_Y);
hY = histogram(Rotation_Y);
grid on
mnYlabel=sprintf('Mean = %5.4f', meanY);
stdYlabel=sprintf('Std Dev = %5.4f', stdY);
delete(h);
h=annotation('textbox',[0.68 0.82 0.1 0.1]);
set(h,'String',{mnYlabel, stdYlabel});
txt = ['\pm ' sprintf('%5.4f', tolY) ' deg'];
text(-.15,650,txt,'FontSize',14,'Color','r')
title('Rotation Y');
xlabel('Variation (deg)');
ylabel('Frequency');
xlim([-.18 .18]);
ylim([0 800]);
line([meanY-tolY,meanY-tolY], ylim, 'Color', 'r',
'LineWidth', 1);
line([meanY+tolY, meanY+tolY], ylim, 'Color', 'r',
'LineWidth', 1);
savename2 = 'histRotY.jpg';
saveas(hY, savename2, 'jpg');

meanZ = mean(Rotation_Z);
hZ = histogram(Rotation_Z);
grid on
mnZlabel=sprintf('Mean = %5.4f', meanZ);
stdZlabel=sprintf('Std Dev = %5.4f', stdZ);
delete(h);
h=annotation('textbox',[0.68 0.82 0.1 0.1]);
set(h,'String',{mnZlabel, stdZlabel});
txt = ['\pm ' sprintf('%5.4f', tolZ) ' deg'];
text(-.025,650,txt,'FontSize',14,'Color','r')
title('Rotation Z');
xlabel('Variation (deg)');
ylabel('Frequency');
xlim([-.027 .027]);
ylim([0 800]);
line([meanZ-tolZ, meanZ-tolZ], ylim, 'Color', 'r',
'LineWidth', 1);
```

```
line([meanZ+tolZ, meanZ+tolZ], ylim, 'Color', 'r',
'LineWidth', 1);
savename3 = 'histRotZ.jpg';
saveas(hZ, savename3, 'jpg');

meanTX = mean(Translation_X);
hTX = histogram(Translation_X);
grid on
mnTXlabel=sprintf('Mean = %3.2f', meanTX);
stdTXlabel=sprintf('Std Dev = %3.2f', stdTX);
delete(h);
h=annotation('textbox',[0.68 0.82 0.1 0.1]);
set(h,'String',{mnTXlabel, stdTXlabel});
txt = ['\pm ' sprintf('%3.2f', tolTX) ' \mum'];
text(-9,650,txt,'FontSize',14,'Color','r')
title('Translation X');
xlabel('Variation (\mum)');
ylabel('Frequency');
xlim([-11 11]);
ylim([0 800]);
line([meanTX-tolTX, meanTX-tolTX], ylim, 'Color', 'r',
'LineWidth', 1);
line([meanTX+tolTX, meanTX+tolTX], ylim, 'Color', 'r',
'LineWidth', 1);
savename4 = 'histTransX.jpg';
saveas(hTX, savename4, 'jpg');

meanTY = mean(Translation_Y);
hTY = histogram(Translation_Y);
grid on
mnTYlabel=sprintf('Mean = %3.2f', meanTY);
stdTYlabel=sprintf('Std Dev = %3.2f', stdTY);
delete(h);
h=annotation('textbox',[0.68 0.82 0.1 0.1]);
set(h,'String',{mnTYlabel, stdTYlabel});
txt = ['\pm ' sprintf('%3.2f', tolTY) ' \mum'];
text(-9,650,txt,'FontSize',14,'Color','r')
title('Translation Y');
xlabel('Variation (\mum)');
ylabel('Frequency');
xlim([meanTY-11 meanTY+11]);
ylim([0 800]);
line([meanTY-tolTY, meanTY-tolTY], ylim, 'Color', 'r',
'LineWidth', 1);
```

```
line([meanTY+tolTY, meanTY+tolTY], ylim, 'Color', 'r',
'LineWidth', 1);
savename5 = 'histTransY.jpg';
saveas(hTY, savename5, 'jpg');

meanTZ = mean(Translation_Z);
hTZ = histogram(Translation_Z);
grid on
mnTZlabel=sprintf('Mean = %5.2f', meanTZ);
stdTZlabel=sprintf('Std Dev = %5.2f', stdTZ);
delete(h);
h=annotation('textbox',[0.68 0.82 0.1 0.1]);
set(h,'String',{mnTZlabel, stdTZlabel});
txt = ['\pm ' sprintf('%4.2f', tolTZ) ' \mum'];
text(276,650,txt,'FontSize',14,'Color','r')
title('Translation Z');
xlabel('Variation (\mum)');
ylabel('Frequency');
xlim([meanTZ-32 meanTZ+32]);
ylim([0 700])
line([meanTZ-tolTZ, meanTZ-tolTZ], ylim, 'Color', 'r',
'LineWidth', 1);
line([meanTZ+tolTZ, meanTZ+tolTZ], ylim, 'Color', 'r',
'LineWidth', 1);
savename6 = 'histTransZ.jpg';
saveas(hTZ, savename6, 'jpg');
```

REFERENCES

[1] K. Maghsoudi, R. Jafari, G. Momen, and M. Farzaneh, "Micro-nanostructured polymer surfaces using injection molding: A review," *Materials Today Communications,* vol. 13, pp. 126-143, 2017/12/01/ 2017, doi: https://doi.org/10.1016/j.mtcomm.2017.09.013.

[2] Y. Byoung Hee, D. S. Park, S. D. Rani, and M. C. Murphy, "Assembly of Polymer Microfluidic Components and Modules: Validating Models of Passive Alignment Accuracy," *Journal of Microelectromechanical Systems,* vol. 24, no. 3, pp. 634-50, 06/ 2015, doi: 10.1109/JMEMS.2014.2339733.

[3] B. H. You, "Microassembly technology for modular, polymer microfluidic devices," Dissertation, Mechanical Engineering, Louisiana State University, LSU Doctoral Dissertations, 2008.

[4] J. Guo, K. Liu, Z. Wang, and G. L. Tnay, "Magnetic field-assisted finishing of a mold insert with curved microstructures for injection molding of microfluidic chips," *Tribology International,* vol. 114, pp. 306-314, 2017/10/01/ 2017, doi: https://doi.org/10.1016/j.triboint.2017.04.019.

[5] J. H. Myung and S. Hong, "Microfluidic devices to enrich and isolate circulating tumor cells," *Lab on a Chip,* vol. 15, no. 24, pp. 4500-11, 12/21 2015, doi: 10.1039/c5lc00947b.

[6] P.-C. Chen *et al.*, "Replication of reliable assembly features for polymer modular microfluidic systems," in *ASME 2007 International Mechanical Engineering Congress and Exposition, IMECE 2007, November 11, 2007 - November 15, 2007*, Seattle, WA, United states, 2007, vol. 11: American Society of Mechanical Engineers (ASME), in ASME International Mechanical Engineering Congress and Exposition, Proceedings (IMECE), pp. 119-124, doi: 10.1115/IMECE200742206. [Online]. Available: http://dx.doi.org/10.1115/IMECE200742206

[7] G. Tosello, F. Marinello, and H. N. Hansen, "Process validation of the injection molding of polymer micro fluidic systems," in *67th Annual Technical Conference of the Society of Plastics Engineers 2009, ANTEC 2009, June 22, 2009 - June 24, 2009*, Chicago, IL, United states, 2009, vol. 5: Society of Plastics Engineers, in Annual Technical Conference - ANTEC, Conference Proceedings, pp. 2584-2591.

[8] Y. Liu, M. C. Song, M. J. Wang, and C. Z. Zhang, "Quality defects and analysis of the microfluidic chip injection molding," in *13th International Manufacturing Conference in China, IMCC2009, September 21, 2009 - September 23, 2009*, Dalian, China, 2009, vol. 628 629: Trans Tech Publications Ltd, in Materials Science Forum, pp. 417-422, doi: 10.4028/www.scientific.net/MSF.628-629.417. [Online]. Available: http://dx.doi.org/10.4028/www.scientific.net/MSF.628-629.417

[9] S. Kuhn, A. Burr, M. Kubler, M. Deckert, and C. Bleesen, "Scratch tests on micro-structured polymer surfaces produced by injection molding and reaction processes," *Journal of Micromechanics and Microengineering,* vol. 21, no. 6, 2011, doi: 10.1088/0960-1317/21/6/065031.

[10] P. Mele and J. Giboz, "Micro-injection molding of thermoplastic polymers: Proposal of a constitutive law as function of the aspect ratios," *Journal of Applied Polymer Science,* vol. 135, no. 4, 2018, doi: 10.1002/app.45719.

[11] P. M. Lambert, E. A. Campaigne Iii, and C. B. Williams, "Design considerations for mask projection microstereolithography systems," in *24th International Solid Freeform Fabrication Symposium - An Additive Manufacturing Conference, SFF 2013, August 12, 2013 - August 14, 2013*, Austin, TX, United states, 2013: University of Texas at Austin (freeform), in 24th International SFF Symposium - An Additive Manufacturing Conference, SFF 2013, pp. 111-130.

[12] I. Gibson, Rosen, David, Stucker, Brent, *Additive Manufacturing Technologies: 3D Printing, Rapid Prototyping, and Direct Digital Manufacturing*, 2nd ed. Springer, 2015.

[13] D. Han, C. Yang, N. X. Fang, and H. Lee, "Rapid multi-material 3D printing with projection micro-stereolithography using dynamic fluidic control," *Additive Manufacturing,* vol. 27, pp. 606-615, 2019, doi: 10.1016/j.addma.2019.03.031.

[14] M. Barraja and R. R. Vallance, "Tolerancing kinematic couplings," *Precision Engineering,* vol. 29, no. 1, pp. 101-112, 2005/01/01/ 2005, doi: https://doi.org/10.1016/j.precisioneng.2004.05.001.

[15] J. Gao, K. W. Chase, and S. P. Magleby, "Generalized 3-D tolerance analysis of mechanical assemblies with small kinematic adjustments," *IIE Transactions,* vol. 30, no. 4, pp. 367-377, 1998/04/01 1998, doi: 10.1080/07408179808966476.

[16] J. Dilag, T. Chen, S. Li, and S. A. Bateman, "Design and direct additive manufacturing of three-dimensional surface micro-structures using material jetting technologies," *Additive Manufacturing,* vol. 27, pp. 167-174, 2019, doi: 10.1016/j.addma.2019.01.009.

[17] M. Barraja, "TOLERANCE ALLOCATION FOR KINEMATIC SYSTEMS," University of Kentucky Master's Theses, 315, 2004. [Online]. Available: https://uknowledge.uky.edu/gradschool_theses/315

[18] B. M. Fabrication. "Materials." https://bmf3d.com/materials/ (accessed 2020).

[19] MIT. "Material Property Database." http://www.mit.edu/~6.777/matprops/pmma.htm (accessed 2020).

[20] designerdata. "PMMA (cast)." https://designerdata.nl/materials/plastics/thermo-plastics/poly(methyl-methacrylate) (accessed 2020.